


Coupled Mo-U abundances and isotopes in a small marine euxinic basin: Constraints on processes in euxinic basins

Journal Article**Author(s):**

Bura-Nakić, Elvira; Andersen, Morten B.; Archer, Corey; [De Souza, Gregory](#) ; Marguš, Marija; Vance, Derek

Publication date:

2018-02-01

Permanent link:

<https://doi.org/10.3929/ethz-b-000211997>

Rights / license:

[Creative Commons Attribution-NonCommercial-NoDerivatives 4.0 International](#)

Originally published in:

Geochimica et Cosmochimica Acta 222, <https://doi.org/10.1016/j.gca.2017.10.023>

1 Coupled Mo-U abundances and isotopes in a small marine
2 euxinic basin: constraints on processes in euxinic basins

3

4 Elvira Bura-Nakic^{1,2}, Morten, B. Andersen^{1,3*}, Corey Archer¹, Gregory F. de
5 Souza¹, Marija Marguš², Derek Vance¹

6

7 ¹Institute of Geochemistry and Petrology, Department of Earth Sciences, ETH Zürich,
8 Clausiusstrasse 25, 8092 Zürich, Switzerland.

9 ²Division for Marine and Environmental Research, Ruđer Bošković Institute, Bijenička 54,
10 HR-10002, Zagreb, Croatia.

11 ³School of Earth and Ocean Sciences, Cardiff University, Cardiff, UK.

12

13 * Corresponding author (andersenm1@cardiff.ac.uk)

14

15 ~9500 words in main text

16 8 figures

17 1 table

18 5 supplementary tables and one supplementary text

19 **Abstract**

20

21 Sedimentary molybdenum (Mo) and uranium (U) abundances, as well as their isotope
22 systematics, are used to reconstruct the evolution of the oxygenation state of the surface Earth
23 from the geological record. Their utility in this endeavour must be underpinned by a thorough
24 understanding of their behaviour in modern settings. In this study, Mo-U concentrations and
25 their isotope compositions were measured in the water column, sinking particles, sediments
26 and pore waters of the marine euxinic Lake Rogoznica (Adriatic Sea, Croatia) over a two year
27 period, with the aim of shedding light on the specific processes that control Mo-U
28 accumulation and isotope fractionations in anoxic sediment.

29 Lake Rogoznica is a 15 m deep stratified sea-lake that is anoxic and euxinic at depth. The
30 deep euxinic part of the lake generally shows Mo depletions consistent with near-quantitative
31 Mo removal and uptake into sediments, with Mo isotope compositions close to the oceanic
32 composition. The data also, however, show evidence for periodic additions of isotopically
33 light Mo to the lake waters, possibly released from authigenic precipitates formed in the upper
34 oxic layer and subsequently processed through the euxinic layer. The data also show evidence
35 for a small isotopic offset ($\sim 0.3\%$ on $^{98}\text{Mo}/^{95}\text{Mo}$) between particulate and dissolved Mo, even
36 at highest sulfide concentrations, suggesting minor Mo isotope fractionation during uptake
37 into euxinic sediments. Uranium concentrations decrease towards the bottom of the lake,
38 where it also becomes isotopically lighter. The U systematics in the lake show clear evidence
39 for a dominant U removal mechanism via diffusion into, and precipitation in, euxinic
40 sediments, though the diffusion profile is mixed away under conditions of increased density
41 stratification between an upper oxic and lower anoxic layer. The U diffusion-driven
42 precipitation is best described with an effective $^{238}\text{U}/^{235}\text{U}$ fractionation of $+0.6\%$, in line with
43 other studied euxinic basins.

44 Combining the Mo and U systematics in Lake Rogoznica and other euxinic basins, it is
45 apparent that the two different uptake mechanisms of U and Mo can lead to spatially and
46 temporally variable Mo/U and Mo-U isotope systematics that depend on the rate of water
47 renewal versus removal to sediment, the sulfide concentration, and the geometry of the basin.
48 This study further emphasises the potential of combining multiple observations, from Mo-U
49 enrichment and isotope systematics, for disentangling the various processes via which redox
50 conditions control the chemistry of modern and ancient sediments.

51

52 **1. Introduction**

53 The sedimentary abundances and isotopic compositions of redox sensitive trace metals play a
54 prominent role in attempts to reconstruct the history of surface Earth oxygenation. Of all the
55 redox sensitive metals that have been used, molybdenum (Mo) and uranium (U) have perhaps
56 been the most prominent. Both are soluble under oxidizing conditions and exhibit
57 conservative behaviour in the open ocean, with residence times that are significantly longer
58 than ocean mixing times (800 and 250–500 kyr respectively, Emerson and Huested, 1991). In
59 some anoxic or euxinic (i.e. anoxic and sulfidic) settings, on the other hand, both Mo and U
60 show non-conservative behaviour in the water column and are variably removed to sediment,
61 though probably via different extraction mechanisms (Ku et al., 1977; Collier, 1985;
62 McLennan, 2001; Algeo and Tribovillard, 2009; Nakagawa et al., 2012; Tribovillard et al.,
63 2012). Organic-rich, reducing sediments are the most important modern oceanic Mo and U
64 sinks (Emerson and Huested, 1991; Morford and Emerson, 1999; McManus et al., 2006; Scott
65 et al., 2008). Coupled analysis of Mo and U authigenic enrichment in reducing organic-rich
66 sediments has been used to investigate the degree of anoxia prevailing in the past water
67 column (e.g., Scott et al., 2008; Algeo and Tribovillard, 2009; Tribovillard et al., 2012).

68 The Mo and parent U isotopic composition of ancient black shales are also thought to be
69 related to the redox state of the global ocean, as Mo and U isotopes are fractionated differently
70 in oxic and anoxic ocean sinks (e.g. Barling et al., 2001; Siebert et al., 2003; Arnold et al.,
71 2004; Stirling et al., 2007; Weyer et al., 2008; Gordon et al., 2009; Montoya-Pino et al., 2010;
72 Scheiderich et al., 2010; Voegelin et al., 2010; Brennecka et al., 2011a; Herrmann et al., 2012;
73 Azrieli-Tal et al., 2014; Dahl et al., 2014; Westermann et al., 2014). The conservative
74 behaviour of Mo in oxygenated waters arises from the fact that the main Mo species,
75 molybdate ($\text{Mo}^{\text{VI}}\text{O}_4^{2-}$), has a low particle affinity, leading to the relatively long residence time
76 of Mo in the oceans (Emerson and Huested, 1991). In such oxidizing environments, slow

77 adsorption of dissolved Mo to Mn oxide particles preferentially accumulates light Mo isotopes
78 in the particulate phase (by $\sim 3\%$ for $^{98}\text{Mo}/^{95}\text{Mo}$; Barling and Anbar, 2004), leaving the
79 dissolved Mo pool enriched in heavy Mo isotopes (Barling and Anbar, 2004). In contrast,
80 under euxinic conditions, with significant dissolved sulfide, oxygen atoms in molybdate can
81 be replaced with sulfur atoms (Erickson and Helz, 2000; Vorlicek and Helz, 2002). The
82 product thiomolybdate ($\text{Mo}^{\text{VI}}\text{O}_n\text{S}_4^{2-}$) species are particle reactive, readily scavenged (e.g. by
83 particulate Fe and organic matter), and thus removed from the water column into the
84 underlying sediments (Helz et al., 1996; Vorlicek and Helz, 2002; Bostick et al., 2003). At
85 sulfide concentrations greater than $\sim 11 \mu\text{mol l}^{-1}$ the conversion of molybdate to
86 tetrathiomolybdate ($\text{Mo}^{\text{VI}}\text{S}_4^{2-}$) is nearly complete (Erickson and Helz, 2000). Thus, in highly
87 restricted anoxic basins, such as the Black Sea ($[\Sigma\text{S}^{\text{II}}] \sim 300 \mu\text{mol l}^{-1}$, Emerson and Husted
88 1991) the conversion of $\text{Mo}^{\text{VI}}\text{O}_4^{2-}$ to $\text{Mo}^{\text{VI}}\text{S}_4^{2-}$ is almost complete at depth, leading to near-
89 quantitative molybdenum removal from the water column. Accordingly, in the underlying
90 sediment, authigenic Mo records a Mo isotopic composition that is very close to the original
91 seawater composition (Nägler et al., 2011). The process of conversion to sulfidic species does,
92 however, involve Mo isotope fractionation (Tossell, 2005; Kerl et al., 2017), which may be
93 expressed in mildly euxinic conditions when intermediate products in the $\text{Mo}^{\text{VI}}\text{O}_4^{2-}$ to
94 $\text{Mo}^{\text{VI}}\text{S}_4^{2-}$ conversion are present and when conversion to tetrathiomolybdate is not complete.
95 Furthermore, there appears to be a small isotopic difference between aqueous $\text{Mo}^{\text{VI}}\text{S}_4^{2-}$ and
96 authigenic solid Mo, with $\Delta^{98/95}\text{Mo}_{\text{tetrathiomolybdate-sediment}} = +0.5 \pm 0.3\%$ (Nägler et al., 2011).

97 Uranium, in the form of U^{6+} , mainly forms highly soluble complexes with carbonate species
98 in oxic seawater, again leading to the relatively long residence time (Morford and Emerson,
99 1999). In contrast, the reduced U^{4+} species is highly insoluble. Large variations in the ratio of
100 uranium's long-lived isotopes $^{238}\text{U}/^{235}\text{U}$ have been observed under redox-controlled U^{6+} - U^{4+}
101 exchange in low-temperature environments (Stirling et al., 2007; Weyer et al., 2008). Oxidic

102 adsorption of U to ferromanganese oxides without redox change, and under oxic conditions,
103 results in a small fractionation of the $^{238}\text{U}/^{235}\text{U}$ ratio ($\delta^{238/235}\text{U}_{\text{soln-MnOx}} = \sim 0.2\%$; Brennecka et
104 al., 2011b). On the other hand, the incorporation of U^{4+} into anoxic sediments generally leads
105 to significant (permil level) enrichment of the heavier isotope, ^{238}U , in sediment (e.g. Weyer
106 et al., 2008; Andersen et al., 2014). In contrast to Mo, typical processes for U removal into
107 anoxic sediments have been suggested to involve U transported with sinking particulate
108 organic matter (Anderson et al. 1989b; Zheng et al., 2002) and diffusion of seawater U into
109 sediment pore waters and reduction within the sediment itself (Anderson et al., 1989a; Barnes
110 and Cochran, 1990; Klinkhammer and Palmer, 1991). Although still a matter of some
111 debate, the latter process has been determined to dominate the authigenic U flux in most
112 studied anoxic marine settings (e.g. Anderson 1987; McManus et al 2005). Furthermore,
113 the mechanistic nature of U fixation within anoxic sediment is also still debated, but
114 likely dominated by metal- and sulfate-reducing bacteria that use U^{VI} as an electron
115 acceptor (Lovley et al., 1991; Bargar et al., 2013).

116 As a result, while the Mo isotopic composition of seawater may be directly recorded in
117 sediments accumulated under strongly euxinic conditions via near-quantitative Mo uptake, U
118 is taken up less quantitatively and U isotopes generally display large fractionations between
119 anoxic organic-rich sediments and seawater (Weyer et al., 2008; Andersen et al., 2014;
120 Noordmann et al., 2015; Holmden et al., 2015; Andersen et al., 2016; Rolison et al., 2017). As
121 Mo and U display significant isotope fractionations between oxic and anoxic sinks, both
122 isotope systems have the potential to record the redox evolution of the global ocean. However,
123 the investigation of Mo and U behaviour in different modern settings has revealed significant
124 Mo isotope fractionation in sediments deposited under suboxic as well as under anoxic water
125 columns bearing low sulfide concentrations (Siebert et al., 2003; Siebert et al., 2006; Poulson
126 et al., 2006; Poulson Brucker et al., 2009; Nägler et al., 2011). In addition to Mo removal in

127 euxinic waters, other processes have been invoked to control sedimentary Mo isotopes in
128 anoxic settings. These include the delivery of Mo with light Mo isotope compositions to
129 euxinic sediments or bottom water on Fe-Mn oxyhydroxide-rich particulates (e.g. Barling
130 and Anbar, 2004; Goldberg et al., 2009), adsorption of Mo to organic matter with an
131 isotopic fractionation (Kowalski et al., 2013) and early diagenetic redistribution of Mo
132 within sediment and pore-waters (McManus et al., 2002). Studies reporting the U isotopic
133 composition of anoxic to suboxic sediments have shown not only a significant U isotopic
134 fractionation in comparison to seawater, but also variable fractionation between these modern
135 anoxic settings. While several studies suggest an apparent U isotope fractionation factor (ϵ)
136 for $^{238}\text{U}/^{235}\text{U}$ in the range of $\sim+0.5$ to 0.8‰ during U uptake in anoxic sediments (Weyer et al.
137 2008; Andersen et al., 2014; Holmden et al., 2015; Noordmann et al., 2015; Andersen et al.,
138 2016, Rolison et al., 2017) both significantly higher and lower U isotope compositions have
139 been observed in anoxic sediments (Weyer et al. 2008; Montoya-Pino et al. 2010; Noordmann
140 et al., 2015; Hinojosa et al. 2016). This suggests further mechanisms for U withdrawal from
141 the anoxic water columns, or variable U isotope mass-balance during non-quantitative
142 authigenic U sediment uptake (Andersen et al., 2017).

143 To improve our understanding of the behaviour of Mo and U and their isotopes, further
144 studies in well-characterised modern settings are needed. In this study, Mo and U
145 concentrations and isotope compositions of the water column, sinking particles, sediments and
146 pore waters of the marine euxinic Lake Rogoznica, Croatia, are presented. Based on the
147 comprehensive dataset obtained, including seasonal patterns, we shed further light on the
148 processes controlling Mo and U isotope fractionation mechanisms in anoxic water columns
149 and their sediments.

150

151 **2. Methods**

152 **2.1. Study site**

153 Lake Rogoznica is a small, intensely eutrophicated sea-lake situated on the eastern coast of
154 the Adriatic Sea (Ciglenečki et al., 2005; Bura-Nakić et al., 2009; Ciglenečki et al., 2015).
155 The lake is surrounded by sheer carbonate cliffs (4–23 m above mean sea-level), has a surface
156 area of about 5300 m² and a maximum depth of ~15 m. Due to its stratification, and despite
157 permanent water exchange with the surrounding sea through porous karst, Lake Rogoznica
158 becomes anoxic at depth due to the remineralisation of organic matter produced in periods of
159 intense primary production (blooms) near the surface (Ciglenečki et al., 2005; Bura-Nakić et
160 al., 2009; Ciglenečki et al., 2015). It is therefore well-suited for studying biogeochemical
161 processes influencing redox-sensitive trace metals. Complete vertical mixing of the lake,
162 where cold oxygen-rich water from the surface mixes downwards and anoxic deep waters are
163 brought to the surface, often occurs during the dry and cold autumn period. Complete mixing
164 of the lake, leading to catastrophic anoxia in the whole water column, occurs rarely, once or
165 twice in every 10 winters depending on the meteorological conditions (Ciglenečki et al., 2005;
166 2015). Under stratified conditions, the surface water is well oxygenated while the layer below
167 approx. 9 m depth is anoxic. The anoxic deep waters become rich in sulfur (up to 5000 μmol l⁻¹
168 ¹) predominantly in the form of sulfide (Ciglenečki et al., 2005; Bura-Nakić et al., 2009;
169 Ciglenečki et al., 2015).

170

171 **2.2. Sampling and sample collection**

172 Prior to field work, syringes, bottles, tygon tubes and all other materials used for sediment and
173 water column sampling were pre-cleaned in ~3 N HCl and rinsed with MQ water (18
174 MΩ·cm). Unless otherwise stated, all reagents used were sub-boiling distilled twice in teflon
175 stills.

176 Water column samples were collected from the middle of the lake during six campaigns
177 spanning 2013 (February, April, July and October) and 2015 (April and July). All water
178 samples were collected by lowering a custom-made (30 cm diameter) filter housing down into
179 the lake, so that filtration occurred *in situ*, and the water was pumped through a 0.2 μm mesh-
180 sized filter (Millipore, Whatman 47 mm diameter PTFE) to the surface using silicone tubing
181 (0.9 cm outer diameter) and a Pegasus peristaltic pump. Approximately one litre was collected
182 at each depth. All filtered samples were collected in pre-cleaned HDPE bottles and acidified
183 (pH 2, using concentrated HCl). Salinity and oxygen concentration were measured *in situ*
184 during the sampling using a HQ40D multimeter probe (HachLange, Germany). Sulfide
185 concentrations were analysed by linear sweep voltammetry (LSV) within 8 hours of sampling
186 according to procedures described elsewhere (Ciglencečki et al., 2005; Bura-Nakić et al., 2009;
187 Ciglencečki et al., 2015). Electrochemical measurements were performed with $\mu\text{Autolab}$
188 Electrochemical Instruments (EcoChemie) connected with 663VA Stand Metrohm electrode.
189 *In situ* measurements of pH were performed during three sampling campaigns (October 2013,
190 April and July 2015) using a HQ40D multimeter probe (HachLange, Germany). The pH
191 values measured *in situ* were used to calculate $[\text{H}_2\text{S}]_{\text{aq}}$ following Millero et al. (1986,
192 Supplementary Table 2).

193 One sediment core (~60 cm long) was collected in July 2013 from the middle and deepest part
194 of Lake Rogoznica (~15 m) using an Uwitec gravity corer. Immediately after sampling, the
195 core was sectioned into 5 cm segments in a glove box under N_2 overpressure. Pore water was
196 extracted by centrifugation at 4000 rpm for 30 minutes. The pore water samples (10 to 30 ml)
197 were transferred into HPDE bottles and acidified (pH 2) using concentrated HCl. A sample of
198 the carbonate rock surrounding the lake was collected in April 2015, stored in a plastic bag,
199 and cut into smaller pieces (1–2 g) using a diamond-blade saw.

200

201 2.3. Sample preparation

202 Chemical preparation and analysis of the samples were performed in the isotope facilities at
203 the Institute of Geochemistry and Petrology, Department of Earth Sciences, ETH Zürich,
204 Switzerland. Lake Rogoznica water column dissolved and particulates, as well as pore water
205 and sediment samples were measured for selected elemental concentrations, and Mo and U
206 isotopes. Elemental concentrations were measured in all samples (section 2.5) prior to
207 preparation for isotope composition determination.

208 Water sample aliquots (varying from 20 to 150 ml) were taken for isotopic analysis, aiming
209 for a total of 20–50 ng U and 150–250 ng Mo. These were transferred into pre-cleaned Teflon
210 jars for the isotope determination, and spiked with the IRMM–3636 ^{236}U – ^{233}U double-spike
211 (Richter et al., 2008) aiming for a $^{236}\text{U}/^{235}\text{U}$ of ~ 4 , and a ^{100}Mo – ^{97}Mo double-spike (Archer
212 and Vance, 2008) aiming for a 1:1 spike to sample ratio. These water sample aliquots were
213 subsequently dried down (all at 100 °C). Due to the high Na–content, a large NaCl precipitate
214 would form during this step. To obtain a more pure metal fraction, samples were leached
215 using 10 ml 7 N HCl for 24 hours, a treatment which dissolves Mo, U and other metals but
216 minimises dissolution of NaCl. The samples were then centrifuged (3500 rpm for 10 minutes),
217 and the supernatant taken for analysis. The recoveries of both U and Mo in the supernatant
218 were consistently >90% using this procedure. The supernatant was then dried down and re-
219 dissolved in 5 ml 7 N HCl in preparation for column chromatography.

220 Filters used for the water filtration were dissolved in 10 ml of concentrated HNO_3 in pre-
221 cleaned 60 ml Teflon beakers and dried down (all at 100 °C). Samples were then re-dissolved
222 and fluxed in a 2 ml mixture of conc. HNO_3 and H_2O_2 (Merck Suprapure, 1:1 ratio) on a
223 hotplate for 24 hours, before being dried down. They were then re-dissolved in 5 ml of 7 N
224 HCl and an aliquot (100 μL) was taken to determine elemental concentrations. The filters held
225 28 to 148 ng Mo and 3 to 23 ng U, while the total blanks for dissolution of clean unused

226 filters in the same manner were ~40 pg for Mo and <1 pg for U (Supplementary Table 1). The
227 samples were spiked with the U and Mo double-spikes as described above, and left in closed
228 Teflon beakers to equilibrate on a hotplate (100 °C) before column chromatography.

229 The pore water samples were weighed, dried down in pre-cleaned Teflon beakers, and pre-
230 treated with the mixture of concentrated HNO₃ and H₂O₂ in a 1:1 ratio on a hotplate for 24
231 hours. Samples were then re-dissolved in 5 ml 7 N HCl and an aliquot taken to determine the
232 elemental concentrations. Samples containing 70–170 ng Mo and 4–35 ng U were then spiked
233 with the U and Mo double-spikes and left to equilibrate on a hotplate in preparation for
234 column chromatography.

235 Approximately 50–100 mg of the sediment samples was used for analysis. Full dissolution of
236 sediments was carried out using conventional protocols for silicates, involving mixtures of
237 HF–HNO₃–HCl and H₂O₂ in the same manner described in Andersen et al. (2013). After final
238 dissolution in 10 ml 6 N HCl, an aliquot was taken to determine elemental concentrations. An
239 aliquot containing 20–50 ng U and 150–250 ng Mo was added to pre-cleaned Teflon beakers,
240 spiked with the U and Mo double-spikes, and then left to equilibrate on a hotplate before
241 being dried down (all at 100 °C). Samples were then re-dissolved in 5 ml 7 N HCl in
242 preparation for column chromatography.

243 The carbonate rock sample was weighed and dissolved in a pre-cleaned Teflon beaker. The
244 initial carbonate rock dissolution was performed in a 5 ml mixture of conc. HCl and H₂O in a
245 1:1 ratio for 24 hours. The sample was then dried down and pre-treated on a hotplate for 24
246 hours with a mixture of conc. HNO₃ and H₂O₂ in a 1:1 ratio. After final dissolution in 10 ml
247 of 0.3 N HNO₃ an aliquot was taken to determine elemental concentrations. An aliquot
248 containing ~50 ng U was added to a pre-cleaned Teflon beaker, spiked with the U double-
249 spike, left to equilibrate on a hotplate before being dried down at 100 °C. The sample was
250 then re-dissolved in 5 ml 7 N HCl in preparation for column chromatography.

251

252 **2.4. Column chromatography**

253 A one step purification and U–Mo separation procedure was conducted using RE Resin
254 (Triskem technologies) in custom-made shrink-fit Teflon columns (~0.2 ml resin reservoir).
255 Prior to sample loading, resin was added to the columns, pre-cleaned using 2 ml of a mixture
256 0.1 N HCl–0.3 N HF, rinsed with MQ water, and pre-conditioned with 2 ml 7 N HCl. Samples
257 were then loaded in 5 ml 7 N HCl and the matrix eluted with 10 ml 1 N HCl. The Mo and U
258 fraction were eluted separately, first with 5 ml 0.2 N HCl and then 5 ml of a 0.1 N HCl–0.3 N
259 HF mixture, respectively. The column chromatography protocol yielded highly pure Mo and
260 U fractions with only traces of major or minor elements. For example, abundant cations in the
261 pre-column extracted seawater – e.g. Mg (~1000 ppm) and Ca (~400 ppm) – were present at
262 less than 100 ppb in the purified Mo and U fractions. Column blanks were <13 pg and <22 pg
263 for Mo and U, respectively (Supplementary Table 1). The U fractions were fluxed on a
264 hotplate for 24 hours in a 1 ml mixture of concentrated HNO₃ and H₂O₂ in 1:1 ratio, to oxidise
265 any resin bleeding into the sample cut during chemistry, and dried down. The purified Mo and
266 U were then re-dissolved in 0.3 N HNO₃ and 0.2 N HCl, respectively, for mass spectrometry.

267 The column separation procedure was tested by processing two open Atlantic Ocean samples
268 for U and Mo, following the dissolution and column chemistry procedure described above.
269 The isotopic compositions of Mo and U measured are in good agreement with previously
270 reported values (see below and Supplementary Table 1) (Siebert et al., 2003; Weyer et al.,
271 2008; Nakagawa et al., 2012; Andersen et al., 2014; Tissot and Dauphas, 2015).

272

273 **2.5. Elemental concentration measurements**

274 The concentrations of selected elements (see Supplementary Table 2) were measured in 0.3N
275 HNO₃ using a Thermo–Finnigan Element XR ICP–MS, following the same measurement
276 protocol as outlined in Andersen et al. (2013, 2016). In brief, the instrument set-up included
277 both low and medium resolution, using a primary in-house concentration standard
278 interspersed with measurements of three unknowns and a secondary standard (BCR–2). The
279 BCR–2 standard was used to monitor the accuracy and reproducibility. Repeated
280 measurements of BCR–2 gave a reproducibility better than ± 10% (1 S.D.) and mean values
281 within ± 10% of the certified concentrations (see Andersen et al., 2016).

282

283 **2.6. Molybdenum and uranium isotope measurements**

284 Isotope ratios were measured on a Neptune (Thermo–Finnigan) MC–ICPMS equipped with
285 an AridusII auto-sampler (CETAC) using a PFA nebulizer and spray chamber (CPI) sample
286 introduction system. Details of instrumental set-up are given in Archer and Vance (2008) for
287 Mo isotopes and Andersen et al. (2016) for U isotopes. Molybdenum isotope ratios are
288 presented as $\delta^{98}\text{Mo} = \left[\frac{{}^{98/95}\text{Mo}_{\text{sample}}}{{}^{98/95}\text{Mo}_{\text{standard}}} - 1 \right] \times 1000$. All Mo isotope compositions for
289 samples are reported relative to NIST SRM 3134 = +0.25‰ (Nägler et al., 2014). Uranium
290 isotope ratios are reported relative to the CRM–145 standard and presented as $\delta^{238}\text{U} =$
291 $\left[\frac{{}^{238/235}\text{U}_{\text{sample}}}{{}^{238/235}\text{U}_{\text{standard}}} - 1 \right] \times 1000$ and as (²³⁴U/²³⁸U) activity ratios compared to secular
292 equilibrium (Cheng et al., 2013).

293 The Mo double spike method was verified via the analysis of an in-house CPI standard as well
294 as open-ocean seawater. During the period of this study, analysis of our in-house CPI standard
295 with standard/spike ratios in the range of 0.1 to 5 gave $\delta^{98}\text{Mo} = -0.02 \pm 0.04\text{‰}$ (all isotope
296 data reported as 2 S.D., Supplementary Table 1) relative to NIST SRM 3134 = +0.25‰. Four
297 seawater samples gave $\delta^{98}\text{Mo}$ of $+2.37 \pm 0.03\text{‰}$, in perfect agreement with previous data for

298 seawater $\delta^{98}\text{Mo}$ (Siebert et al., 2003; Nakagawa et al., 2012). The verification of the U double
299 spike method was carried out via repeated measurements of the in-house CZ-1 uraninite
300 standard and five open-ocean seawater samples (Supplementary Table 1). The long-term
301 average and ± 2 S.D. reproducibility for the CZ-1 standard were $-0.04 \pm 0.07\text{‰}$ for $\delta^{238}\text{U}$ and
302 0.9996 ± 0.0025 for ($^{234}\text{U}/^{238}\text{U}$) (Supplementary Table 1), in agreement with previously
303 reported values (Stirling et al., 2007; Andersen et al., 2015; 2016). Uranium isotopic analysis
304 of five seawater samples gave a $\delta^{238}\text{U} = -0.39 \pm 0.04\text{‰}$ and ($^{234}\text{U}/^{238}\text{U}$) = 1.147 ± 0.003 ,
305 again in very good agreement with reported data for seawater (Weyer et al., 2008; Andersen et
306 al., 2010; 2014; Tissot and Dauphas, 2015). Finally, a set-up measuring samples with low U
307 (2–10 ng) amounts equivalent to some filter samples, yielded $\delta^{238}\text{U} = -0.02 \pm 0.23\text{‰}$ and
308 ($^{234}\text{U}/^{238}\text{U}$) = 0.999 ± 0.018 for the CZ-1 standard (Supplementary Table 1).

309

310 **3. Results**

311 **3.1. General chemical characterisation of the water column**

312 Salinity, oxygen ($[\text{O}_2]$), sulfide ($[\Sigma\text{S}^{\text{II}}]$), particulate Fe ($[\text{Fe}]_{\text{part}}$) and particulate Mn ($[\text{Mn}]_{\text{part}}$)
313 in the water column are presented in Supplementary Table 2 and summarised in Figure 1.
314 During the study period (2013 and 2015) the lowest salinity recorded was during winter and
315 spring due to increased precipitation and decreased evaporation during the colder season of
316 the year. The position of the halocline is temporally variable, from approx 5 to 9 m. Oxygen
317 concentrations are strongly inversely correlated with the $[\Sigma\text{S}^{\text{II}}]$, the latter reaching the highest
318 concentration of $\sim 5 \text{ mmol l}^{-1}$ in summer 2013 at 13 m depth. Particulate Fe and Mn are higher
319 at the chemocline and in the deeper anoxic waters than in the upper oxic layer.

320

321 **3.2. Molybdenum in the water column and settling particles**

322 Depth profiles of salinity-normalised (to 35) dissolved Mo ($[\text{Mo}]_{\text{SNdiss}}$) and of particulate Mo
323 ($[\text{Mo}]_{\text{part}}$), as well as their $\delta^{98}\text{Mo}$, are presented in Supplementary Table 2 and Figure 2. The
324 $[\text{Mo}]_{\text{SNdiss}}$ is higher than the measured $[\text{Mo}]$ by 3 to 50% in the upper oxic waters ($\text{O}_2 > 5 \text{ mg}$
325 l^{-1}) that are influenced by precipitation, but the correction has little impact on the deeper
326 anoxic waters. The $[\text{Mo}]_{\text{SNdiss}}$ profiles show a strong depth gradient, mirroring changes in the
327 redox conditions in the water column. With the exception of very high $[\text{Mo}]$ in surface waters
328 in April and July 2013, $[\text{Mo}]$ generally varies between $\sim 100 \text{ nmol l}^{-1}$ in the oxic and $\sim 10 \text{ nmol}$
329 l^{-1} in the deeper euxinic waters. The shape of the profiles is rather different for the first three
330 sampling dates (February-July 2013) versus the last three (Oct 2013, April 2015, July 2015).
331 The latter three profiles show a much sharper transition across the chemocline and much more
332 homogeneous concentrations within each redox regime – the upper oxic layer and the lower
333 euxinic layer. For the later three sampling times, $[\text{Mo}]_{\text{part}}/[\text{Mo}]_{\text{diss}}$ is homogeneously low in
334 the upper oxic water column (generally ≤ 0.01) and higher in the lower anoxic portion (up to
335 0.19). The first three sampling events are also much more heterogeneous in this ratio.

336 Lake Rogoznica waters generally show dissolved Mo isotopic composition ($\delta^{98}\text{Mo}_{\text{diss}}$) in
337 the range +2.2 to +2.5 ‰ (Fig. 2). The exception is April 2013 and the top of the water
338 column in July 2013, where values are much more variable and extend down to +0.8‰.
339 The isotopic composition of the particulate Mo ($\delta^{98}\text{Mo}_{\text{part}}$) spans a wide range, from
340 $\delta^{98}\text{Mo} = +0.1$ to +2.1‰. In the anoxic water column the particles were generally more
341 enriched in heavy Mo isotopes ($\delta^{98}\text{Mo}_{\text{part}}$ from +0.6 to +2.0‰) in comparison with those
342 from the oxic water column (from +0.1 to +1.8‰).

343

344 **3.3. Uranium in the water column and settling particles**

345 Salinity normalised ($[U]_{\text{SNdiss}}$) and particulate ($[U]_{\text{part}}$) U concentrations, as well as $\delta^{238}\text{U}$,
346 are presented in Supplementary Table 3 and Figure 2. As with Mo, the salinity
347 normalisation increases the $[U]_{\text{SNdiss}}$ by 2 to 50% in the upper oxic waters influenced by
348 precipitation, but has little influence on the deeper high salinity anoxic waters. The deeper
349 anoxic waters are depleted in dissolved U ($[U]_{\text{diss}}$: 1.4 to 3.4 nmol l⁻¹) compared to the
350 oxic surface layer (8.9 to 11.2 nmol l⁻¹). Dissolved $[U]$ decreases towards the bottom for all
351 6 sampling campaigns. Particulate U concentrations (normalised to the water volume the
352 filters were extracted from) are generally low, ranging from 0.01 to 0.1 nmol l⁻¹ during
353 the whole sampling period, and show no significant seasonal variation. Particulate U
354 concentrations are consistently higher within the anoxic waters column, reaching a
355 maximum at the chemocline and the bottom of the lake. The $[U]_{\text{part}}/[U]_{\text{diss}}$ is significantly
356 lower than the $[\text{Mo}]_{\text{part}}/[\text{Mo}]_{\text{diss}}$ ratio, reaching max values of 0.004 for the oxic water column
357 and 0.03 for anoxic water column samples.

358 Data for the uranium isotopic composition of the dissolved pool ($\delta^{238}\text{U}_{\text{diss}}$) show lighter
359 values than that for open-ocean seawater ($\delta^{238}\text{U} = -0.39\text{‰}$, Supplementary Table 1),
360 ranging from -0.5 to -1.1‰ and with generally lower values with depth. The isotopic
361 composition of particulate U ($\delta^{238}\text{U}_{\text{part}}$) is in the range -0.2‰ to -1.5‰ , with the lowest
362 $\delta^{238}\text{U}_{\text{part}}$ recorded in July 2013 at 6m depth, near the chemocline. $(^{234}\text{U}/^{238}\text{U})_{\text{diss}}$ was in the
363 range 1.111 to 1.148 and $(^{234}\text{U}/^{238}\text{U})_{\text{part}}$ in the range 1.101 to 1.152 (Supplementary Table
364 3).

365

366 **3.4. Molybdenum and uranium in the sediments and pore water**

367 Mo and U concentrations ($[\text{Mo}]_{\text{bulk}}$, $[\text{U}]_{\text{bulk}}$) and isotopic compositions ($\delta^{98}\text{Mo}_{\text{bulk}}$,
368 $\delta^{238}\text{U}_{\text{bulk}}$) in the anoxic sediments are presented in Supplementary Table 4 and Fig. 3.

369 These bulk data were used to calculate authigenic abundances using the measured Al, Mo and
 370 U in the sediment samples (Supplementary Table 4) and assumed lithogenic Mo/Al and U/Al
 371 ratios of $1.1 \times 10^{-5} \text{ g g}^{-1}$ and $1.8 \times 10^{-5} \text{ g g}^{-1}$, respectively (Taylor and McLennan, 1985;
 372 Tribovillard et al., 2006; Andersen et al., 2014). For the isotopic composition of the detrital
 373 component a $\delta^{98}\text{Mo}_{\text{det}}$ of +0.3‰ (Voegelin et al., 2014) and a $\delta^{238}\text{U}_{\text{det}}$ of -0.3‰ (Andersen et
 374 al., 2016), were used, with:

375

$$376 \quad \delta^{98}\text{Mo}_{\text{auth}} = \frac{(\delta^{98}\text{Mo}_{\text{bulk}}[\text{Mo}]_{\text{bulk}} - \delta^{98}\text{Mo}_{\text{det}}[\text{Mo}]_{\text{det}})}{[\text{Mo}]_{\text{auth}}} \quad [1]$$

377

$$378 \quad \delta^{238}\text{U}_{\text{auth}} = \frac{(\delta^{238}\text{U}_{\text{bulk}}[\text{U}]_{\text{bulk}} - \delta^{238}\text{U}_{\text{det}}[\text{U}]_{\text{det}})}{[\text{U}]_{\text{auth}}} \quad [2]$$

379

380 Using this approach, the detrital Mo contribution to the sedimentary budget is found to be
 381 minimal, so that more than 99% of the Mo in the sediments has an authigenic origin. Thus, the
 382 impact of the detrital fraction on the measured bulk Mo isotopic composition of the sediment
 383 is also negligible. For the bulk U there is a higher contribution of detrital U (from 10 to 23%).
 384 Accordingly, the calculated authigenic $\delta^{238}\text{U}$ is shifted towards slightly lower values (by up to
 385 0.03‰) relative to the bulk sediment. The measured ($^{234}\text{U}/^{238}\text{U}$) ratio in the samples, along
 386 with an assumption that the detrital material is in secular equilibrium (~ 1) and that the
 387 authigenic U has a ratio = 1.147 like modern seawater, provides an alternative method for
 388 performing the detrital U correction. The sediments display high ($^{234}\text{U}/^{238}\text{U}$), ranging from
 389 1.096 to 1.120, demonstrating the predominance of authigenic U. Removal of the detrital U

390 component from the bulk using ($^{234}\text{U}/^{238}\text{U}$), leads to corrected $\delta^{238}\text{U}$ authigenic values that are
391 essentially the same as those obtained using the U/Al method (see Supplementary Table 4).

392 The $[\text{Mo}]_{\text{auth}}$ and $[\text{U}]_{\text{auth}}$ were in the range 11 to 80 $\mu\text{g g}^{-1}$ and 2.4 to 7.3 $\mu\text{g g}^{-1}$,
393 respectively, implying moderate Mo and U enrichments in the anoxic sediments. The
394 $\delta^{98}\text{Mo}_{\text{auth}}$ is variable (1.6 to 2.2‰), but is consistently lower than the average oceanic
395 $\delta^{98}\text{Mo}$ composition ($+2.36 \pm 0.10\text{‰}$, Siebert et al., 2003). Sedimentary $\delta^{238}\text{U}_{\text{auth}}$ is, on
396 average, slightly higher ($\sim 0.15\text{‰}$) than the average oceanic $\delta^{238}\text{U}$ (-0.39‰), with the
397 exception of the sample from 17.5 cm ($\delta^{238}\text{U}_{\text{auth}} = -0.42 \pm 0.07\text{‰}$). The sedimentary
398 ($^{234}\text{U}/^{238}\text{U}$) shows no significant variability throughout the investigated core
399 (Supplementary Table 4). The measured host carbonate rock sample gave a $\delta^{238}\text{U} = -0.16$
400 $\pm 0.04\text{‰}$, a ($^{234}\text{U}/^{238}\text{U}$) of 1.012, a $[\text{U}]_{\text{bulk}}$ of 1.12 $\mu\text{g g}^{-1}$ and $[\text{Mo}]_{\text{bulk}}$ of 0.72 $\mu\text{g g}^{-1}$
401 (Supplementary Table 4).

402 Pore water Mo and U concentrations ($[\text{Mo}]_{\text{pw}}$, $[\text{U}]_{\text{pw}}$) (Supplementary Table 5, Fig. 3)
403 were consistently low throughout the core, with average $[\text{Mo}]_{\text{pw}} = 5 \pm 1 \text{ nmol l}^{-1}$ and $[\text{U}]_{\text{pw}}$
404 $= 0.17 \pm 0.04 \text{ nmol l}^{-1}$ (n=13). The $\delta^{238}\text{U}_{\text{pw}}$ closely resembles the $\delta^{238}\text{U}_{\text{diss}}$ recorded in the
405 deepest anoxic bottom waters ($\delta^{238}\text{U}_{\text{diss}}$ in the range -0.9 to -1.1‰). In contrast, pore
406 water Mo is slightly enriched in the heavier Mo isotopes, with an average $\delta^{98}\text{Mo}_{\text{pw}}$ of
407 $+2.48 \pm 0.08\text{‰}$ (n=13), in comparison to $\delta^{98}\text{Mo}_{\text{diss}}$ in anoxic bottom waters (see Figures 2
408 and 3).

409

410 **4. Discussion**

411 **4.1 Behaviour of Mo and its isotopes in Lake Rogoznica**

412 **4.1.1 Water column Mo behaviour**

413 The depth profiles for Mo and its isotopes in Fig. 2 split into two types of behaviour. The
414 dissolved Mo concentration profiles for October 2013 to July 2015 closely resemble those
415 previously reported from Lake Rogoznica (Helz et al., 2011), in showing a sharp transition
416 across the chemocline from high in the oxic portion above to low in the anoxic part of the lake
417 below. Profiles between Feb 2013 and July 2013, on the other hand, show more unexpected
418 behaviour. Below we discuss these anomalous features first, before moving on to the more
419 “typical” features of the later three sampling campaigns.

420 The first three sampling campaigns, and in particular April and July 2013, are often
421 characterised by very high Mo concentrations ($[\text{Mo}]_{\text{SN}}$ up to 577 nmol l^{-1}) in oxic surface
422 waters. (Fig. 2). Moreover, although these profiles exhibit the expected decrease of dissolved
423 Mo in anoxic waters, concentrations at depth are up to 2.5 times higher than in the later three
424 sampling campaigns. These high dissolved Mo concentrations are associated with generally
425 lower $\delta^{98}\text{Mo}_{\text{diss}}$, both in the oxic upper water column (as low as $+0.75 \pm 0.02\text{‰}$) and in the
426 deep euxinic portion (as low as $+1.32 \pm 0.02\text{‰}$). Combined, these observations suggest an
427 additional source of isotopically light Mo to the water column before or during this period.
428 For the oxic part of the water column, the Mo abundance and isotopic data are mostly
429 explained by the mixing of a “normal” signature, typified by the analyses from October 2013
430 to July 2015, with an additional Mo source that has a $\delta^{98}\text{Mo}$ of around $+0.4$ to $+0.5\text{‰}$ (Fig.
431 4a).

432 The origin of this additional Mo source is more difficult to identify. The Mediterranean
433 generally sees unusually high dust supply from the Sahara (Prospero, 1996), and one
434 possibility is that the additional Mo derives from such a source. The Mo associated with dust
435 is most likely to be associated with Fe-Mn oxyhydroxide-rich surfaces, which have the
436 required light isotope compositions (e.g. Barling and Anbar, 2004; Goldberg et al., 2009).
437 It is notable that the reservoir of Mo in particulates is also high, by one or two orders of

438 magnitude, during the anomalous sampling periods. The $\delta^{98}\text{Mo}_{\text{part}}$ is also consistently lower
439 than during the last three sampling campaigns, particularly in the upper oxic water
440 column where the difference between the dissolved and particulate loads ($\Delta^{98}\text{Mo}_{\text{diss-part}}$) is
441 up to +2.2‰ in the first three samplings versus a maximum of +1.3‰ in the second three.
442 The suggested dust source is not strongly supported by particulate Al, Fe and Mn
443 concentrations which, though variable through time and space, are not particularly
444 strongly correlated with high Mo concentrations or light Mo isotopes. On the other hand,
445 if dust particles fall quickly through the water column while their impact lingers in the
446 dissolved pool, or if Mo on Fe-Mn coatings is particularly soluble relative to Fe and Mn,
447 such a correlation might not necessarily be expected.

448 Another potential Mo source could, in principle, be leaching of Mo from the surrounding
449 carbonate karst. However, Mo concentration in the carbonate rock sample measured was
450 low ($0.71 \mu\text{g g}^{-1}$, Supplementary Table 4), in agreement with previously reported values
451 for carbonate (Vogelin et al., 2009, 2010). The main reservoir of Mo in the carbonate host
452 rock is also likely to be Fe-Mn oxyhydroxide coatings. The vertical position of the
453 halocline in Lake Rogoznica shifts seasonally, and during winter 2013 it was situated at a
454 relatively shallow level (3 to 4 m depth). This may have allowed anoxic waters to enter
455 into karst channels and dissolve Fe-Mn oxyhydroxide coatings on carbonate. Finally, the
456 vertical position of the chemocline in Lake Rogoznica also varies, by 2-4m, again
457 depending on season and meteorological conditions. Such temporal variation may also
458 periodically expose Mo sequestered to Fe-Mn oxyhydroxides, in recently deposited
459 unconsolidated sediment in the oxic portion of the lake, to reductive dissolution.

460 During the last three sampling campaigns dissolved salinity-normalised Mo
461 concentrations in the upper 5m of the water column are, at $97 \pm 5 \text{ nmol kg}^{-1}$, close to the
462 mean oceanic $[\text{Mo}]_{\text{diss}}$ value ($107 \pm 7 \text{ nmol l}^{-1}$, Collier, 1985; Nakagawa et al., 2012). In

463 addition, the average $\delta^{98}\text{Mo}_{\text{diss}}$ for these samples is +2.16 to 2.34‰, similar to the
464 measured average oceanic dissolved pool $\delta^{98}\text{Mo}$ signature ($\delta^{98}\text{Mo} = +2.37 \pm 0.03\text{‰}$,
465 Supplementary Table 1). The $\delta^{98}\text{Mo}_{\text{part}}$ ranged from +0.98 to +1.68‰ in the oxic surface
466 waters and $\delta^{98}\text{Mo}_{\text{diss-part}} = 0.65\text{-}1.53\text{‰}$. This difference is consistent with a dominant role for
467 amorphous Fe (oxyhydr)oxides (e.g. ferrihydrite, goethite), which have been shown
468 experimentally to exhibit fractionations relative to dissolved Mo in the range of 1.1 to 1.4‰
469 (Goldberg et al., 2009).

470 At the chemocline, $[\text{Mo}]_{\text{diss}}$ decreases and reaches steady concentrations of about 9 nmol
471 l^{-1} in the anoxic ($\text{O}_2 \sim 0 \text{ mg l}^{-1}$) waters below, a behaviour previously observed both at
472 Lake Rogoznica (Helz et al., 2011), and in other modern euxinic basins (Emerson and
473 Husted, 1991; Colodner et al., 1995; Algeo and Tribovillard, 2009; Nägler et al., 2011). In
474 all the profiles there are minor but significant excursions in $\delta^{98}\text{Mo}$ of the dissolved pool
475 close to the chemocline. For example, in October 2013 and April 2015, $\delta^{98}\text{Mo}_{\text{diss}}$ shows a
476 slight increase, by about 0.3‰, just at and below the chemocline and at depths where
477 significant removal of dissolved Mo starts. Just beneath this, $\delta^{98}\text{Mo}_{\text{diss}}$ decreases again
478 and the deepest samples are again close to those in oxic waters, at $\delta^{98}\text{Mo}_{\text{diss}} =$
479 $+2.31 \pm 0.14\text{‰}$. The July 2015 campaign does not record the initial increase as Mo
480 concentrations begin to drop with depth. Particulate Mo concentrations increase beneath
481 the chemocline, and though they stay beneath 2 nmol l^{-1} , the $[\text{Mo}]_{\text{part}}/[\text{Mo}]_{\text{diss}}$ ratio
482 increases to values as high as 0.2. The $\Delta^{98}\text{Mo}_{\text{diss-part}}$ decreases with depth, with $\delta^{98}\text{Mo}_{\text{part}}$
483 compositions up to +2.03‰ in the deeper anoxic water column.

484 To our knowledge, the only other study reporting $\delta^{98}\text{Mo}$ values for sinking particles
485 formed in anoxic water columns is that for Lake Cadagno, Switzerland, in Dahl et al.
486 (2010). This study hypothesised that $\Delta^{98}\text{Mo}_{\text{diss-part}}$ in anoxic waters is a function of both

487 $[H_2S]_{aq}$ and the time available for equilibration between particles and water versus the
488 scavenging lifetimes of intermediate thiomolybdate species. In this view, when sulfide
489 levels are low enough for non-quantitative transformation of molybdate to
490 tetrathiomolybdate, and for rapid scavenging timescales for intermediate thiomolybdate
491 species, isotopic differences are expected between residual dissolved Mo and particulate
492 Mo (Tossell, 2005; Kerl et al., 2017).

493 Consistent with this view, the data for $\Delta^{98}Mo_{diss-part}$ within the water column of Lake
494 Rogoznica does exhibit a strong relationship with total dissolved sulfide (Fig. 4b). But
495 the relationship appears to become asymptotic to a value of about +0.3‰ at very high
496 dissolved sulfide levels. It is possible that general conclusions regarding the behaviour of
497 Mo and its isotopes in euxinic water columns from these Lake Rogoznica data are
498 complicated by the potential impact of Fe-Mn oxyhydroxide particulates, discussed
499 earlier with reference to the first three sampling campaigns. For example, it is possible
500 that the small excursions near the chemocline could be caused by oxidative-reductive
501 cycle involving Fe-Mn oxyhydroxides. Such a rationale is not, however, consistent with
502 all the details of the data. Thus, the small increase in $\delta^{98}Mo_{diss}$ just below the chemocline,
503 where Mo is first removed from the water column, is the opposite to that which might be
504 expected if isotopically light Fe-Mn oxyhydroxides were sinking into the euxinic layer
505 and undergoing reductive dissolution. Rather this feature, coupled to increases in the
506 Mo_{part}/Mo_{diss} ratio, is much more readily explained in terms of preferential and non-
507 quantitative removal of light Mo isotopes to particulates due to formation of intermediate
508 thiomolybdates at low dissolved sulfide concentrations. Thus, although the exact value of
509 $\Delta^{98}Mo_{diss-part}$ in the anoxic water column is difficult to estimate from our data set, it is
510 very likely that the removal of Mo from the anoxic water of Lake Rogoznica is associated

511 with minor Mo isotope fractionation, similar to that already observed in Kyllaren Fjord,
512 Black and Baltic Sea anoxic water columns (Nägler et al., 2011; Noordmann et al., 2015).

513

514 ***4.1.2 Mo and its isotopes in sediment and pore water***

515 As noted in Section 3, the detrital Mo component of anoxic Lake Rogoznica sediments is very
516 small, and more than 99% has an authigenic origin. The overall $\delta^{98}\text{Mo}_{\text{auth}}$ is high (Fig. 3),
517 ranging from +1.6 to +2.2‰, and with an average of $1.95 \pm 0.17\text{‰}$, (n=13, 1SD). The
518 dissolved-particulate difference for sediment-pore water pairs shows a more scattered
519 relationship with total dissolved sulfide than data for the water column (Fig. 4b). It is
520 again the case, however, that $\Delta^{98}\text{Mo}_{\text{diss-part}}$ is never zero, and the minimum values
521 observed are again about 0.3‰, similar to the water column. This overall finding is again
522 consistent with the previous suggestion in Nägler et al. (2011) that $\Delta^{98}\text{Mo}_{\text{diss-part}}$, even for
523 near-quantitative removal to sediment at high sulfide concentrations, does involve a small
524 fractionation.

525 On the other hand, sediments at Lake Rogoznica are again more complicated than such a
526 simple picture can explain. Dissolved sulfide levels in the pore waters of Lake Rogoznica
527 are very high, and equilibration times in the sediment are presumably long. Thus, the
528 occasionally high values of $\Delta^{98}\text{Mo}_{\text{diss-part}}$ are difficult to explain without invoking some
529 temporal variation in redox conditions. Most of the time, Lake Rogoznica waters are
530 characterised by a sharp chemical gradient and an anoxic layer with high $[\text{H}_2\text{S}]_{\text{aq}}$ at
531 depths >8–9 m, but seasonal mixing is known to occur during particularly dry and cold
532 autumn periods (Ciglencečki et al., 2005; Helz et al., 2011; Ciglencečki et al., 2015).
533 During these periods cold oxygenated waters slowly sink towards the bottom, causing
534 contraction of the anoxic layer so that anoxic conditions are restricted to the deep

535 nepheloid layer (~13 m, Helz et al., 2011). The last two such complete mixing events
536 occurred in 2011 and 1997 (Ciglenc̆ki et al., 2005; Ciglenc̆ki et al., 2015). After these
537 events, anoxia is re-established, potentially causing reductive dissolution of Fe-Mn
538 (oxyhydr)oxides deposited at the bottom of the lake during mixing events (Helz et al.,
539 2011). We speculate that, after these events, Lake Rogoznica bottom waters are most
540 probably enriched in light Mo isotopes, which could potentially affect the isotopic
541 composition of Mo extracted from such waters.

542

543 **4.2 Behaviour of U and its isotopes in Lake Rogoznica**

544 ***4.2.1 Uranium and its isotopes in the water column***

545 Previous studies from the two major modern semi-restricted euxinic basins (Cariaco Basin
546 and Black Sea) have suggested that in such settings U is not removed to sediment through
547 processes in the water column, but rather via reduction in sediment driving U diffusion from
548 the overlying waters into the sediments (Anderson, 1987; Anderson et al., 1989a). The first-
549 order features of the Lake Rogoznica data can first be assessed in terms of this paradigm, in
550 the interests of ascertaining whether it is generally applicable to euxinic basins of different
551 sizes and, for example, at the very high dissolved sulfide concentrations seen in Lake
552 Rogoznica.

553 Focusing first on U concentration, the above scenario implies no removal term in the water
554 column, so that water column depth profiles should be explained in terms of diffusion and
555 advection processes alone. In a simplified diffusion-advection-reaction framework the precise
556 shapes of [U] depth profiles will be dependent on the rate of U diffusion into sediment
557 compared to the rate at which the water column is mixed by advection. Here we assess

558 whether such a simplified model explains the first order features of the [U] data for Lake
559 Rogoznica.

560 At steady-state, any depth profile in the lake can be modelled using the ADR equation:

561

$$562 \quad D_z \frac{d^2C}{dz^2} - \omega_z \frac{dC}{dz} - kC = 0 \quad [3]$$

563 where z is depth, D is the rate of diffusion, ω is the rate of advection and k is a rate constant
564 for removal *within* the water column. If there is no removal within the water column ($k = 0$),
565 the solution to equation [3] for boundary conditions $C(z) = C_0$ at $z = 0$ (lake surface) and $C(z)$
566 $= C_m$ at $z = m$ (lake bottom) is:

$$567 \quad C(z) = C_0 + (C_m - C_0) \frac{e^{\frac{\omega_z z}{D_z}} - 1}{e^{\frac{\omega_z z_m}{D_z}} - 1} \quad [4]$$

568

569 By setting suitable [U] at the top (C_0) and bottom (C_m), model depth profiles can be compared
570 to the data.

571 The depth profiles for [U] from the different sampling campaigns (Fig. 2,5A) vary between
572 those that are close to continuous U depletion profiles with increasing depth (diffusion-
573 dominated), versus others suggesting a very strong chemocline separating well-mixed upper
574 and lower layers (advection dominated within each layer, diffusion across the chemocline).

575 For example, the entire [U] depth profiles from the early sampling campaigns (e.g. February
576 2013) can be modelled in terms of processes dominated by diffusion downwards into the
577 sediment (Fig. 5), with no requirement for removal or addition (no reaction term) within the
578 water column. The later sampling campaigns, where a more stratified water column develops,

579 better approximate to two well-mixed reservoirs above and below the chemocline, with more
580 limited mass transfer between (e.g. July 2015; Fig. 5). This type of profile requires advective
581 mixing within the upper and lower layer, coupled to slower diffusive transport across the
582 chemocline, but is also completely consistent with the lack of a removal term within the water
583 column.

584 Overall, then, the first order features for the water-column dissolved pool uranium
585 concentrations require no removal within the water column, consistent with earlier
586 conclusions for the Black Sea and Cariaco Basin that U removal occurs within sulfidic
587 sediments (Anderson, 1987; Anderson et al., 1989a). Further, more detailed, constraints on the
588 U removal process come from water column U isotopes. Uranium isotope fractionation occurs
589 during the U(VI) to U(IV) transition, as evidenced by theoretical equilibrium calculations (e.g.
590 Bigeleisen 1996) and abiotic and biotic experiments (e.g. Basu et al., 2014; Stylo et al., 2015;
591 Stirling et al., 2015; Wang et al., 2015). The overall isotope fractionation associated with
592 uranium reduction is about 1-1.3 ‰, with the heavy isotope preferred in the reduced species
593 (e.g. Bigeleisen, 1996; Fujii et al., 2006; Abe et al., 2008, 2010). In the modern euxinic Black
594 Sea, $\delta^{238}\text{U}$ in sediments is generally around 0.4 ‰ higher than the open ocean value, while the
595 deeper water column is driven to lower $\delta^{238}\text{U}$ (Weyer et al. 2008; Andersen et al. 2014;
596 Rolison et al. 2017). Previously (Andersen et al. 2014) these data were explained in terms of
597 an effective U isotope fractionation of +0.6‰, i.e. about half the full fractionation, due to U
598 uptake and precipitation in sediments driven by diffusion from overlying seawater and
599 transport-diffusion limitation in the pore water-sediment (e.g. Bender, 1990; Clark and
600 Johnson 2008).

601 If U removal occurs in this manner, the faster removal of ^{238}U than ^{235}U into the sediment
602 should lead to systematically lower $\delta^{238}\text{U}$ in the waters above and must occur in a manner that
603 is consistent with the 0.6‰ difference in the sequestration of ^{238}U relative to ^{235}U (see

604 supplementary text for details). On the other hand, if U were to be removed via reduction in
 605 the water column itself with no transport-diffusion limitation, the U isotope fractionation
 606 process is expected to produce water column $\delta^{238}\text{U}$ values that reflect the full ~ 1.2 ‰
 607 fractionation. At steady state, the overall input of U and its isotopes to Lake Rogoznica from
 608 the open sea must equal the outputs, i.e. outflow of water from the lake to the ocean, and
 609 output to sediment:

610

$$611 \quad C^{\text{ocean}} F_{\text{exch}} - C^{\text{lake}} F_{\text{exch}} - k C^{\text{lake}} = 0 \quad [5]$$

612

613 Where C^x is [U] in the ocean or lake, F_{exch} is the water exchange rate and k is a rate constant
 614 for removal of U to sediment. Rearranging:

615

$$616 \quad C^{\text{lake}} = F_{\text{exch}} \frac{(C^{\text{ocean}} - C^{\text{lake}})}{k} \quad [6a]$$

617

618 The above is also true for each of ^{238}U and ^{235}U so that:

619

$$620 \quad C_{238}^{\text{lake}} = F_{\text{exch}} \frac{(C_{238}^{\text{ocean}} - C_{238}^{\text{lake}})}{k_{238}} \quad \text{and} \quad C_{235}^{\text{lake}} = F_{\text{exch}} \frac{(C_{235}^{\text{ocean}} - C_{235}^{\text{lake}})}{k_{235}} \quad [6b]$$

621

622 Combining [6a] and [6b]:

623

624
$$\frac{C_{238}^{\text{lake}}}{C_{235}^{\text{lake}}} = \frac{k_{235}}{k_{238}} \left(\frac{C_{238}^{\text{ocean}} - C_{238}^{\text{lake}}}{C_{235}^{\text{ocean}} - C_{235}^{\text{lake}}} \right) \quad [7]$$

625

626 Thus, at steady state the average $^{238}\text{U}/^{235}\text{U}$ ratio of the lake is independent of the relative sizes
 627 of the uranium fluxes, and depends only on the isotopic composition of the output to sediment
 628 and the degree to which the lake water is modified between input and output.

629 For Lake Rogoznica, potential scenarios can be examined with the above model of steady
 630 state U removal and the $\delta^{238}\text{U}$ vs [U] systematics (Fig. 6). The ultimate input of U may be
 631 approximated by the open ocean, with $\delta^{238}\text{U}$ of -0.4 ‰ and [U] of 13.4 nM. Though this may
 632 be slightly modified during transport through the karst, the ($^{234}\text{U}/^{238}\text{U}$) in the lake water is
 633 close to the open ocean value, suggesting this effect is minor. Fig. 6 shows all the water
 634 column data for all sampling campaigns. Clearly, though the data lie closer to the diffusion-
 635 driven U removal model (solid line in Fig 6A, $k_{235}/k_{238} = 0.9994$) than one involving
 636 irreversible removal in the water column (dashed line in Fig 6A, $k_{235}/k_{238} = 0.9988$), there is
 637 also considerable scatter. Some of this scatter is, however, readily explainable once more in
 638 terms of the relative importance of diffusion and advection, with little requirement for
 639 reaction within the water column. Thus, for example, data for February 2013 again
 640 approximate most closely a situation where diffusion occurs into the sediment across the
 641 whole depthscale of the lake (Fig. 6A). But where stratification of the lake occurs, again
 642 typified by July 2015 (Fig. 6C), it is only the lower anoxic portion of the lake that
 643 approximates the model for diffusion into sediment, whereas the well-mixed upper portion of
 644 the lake, now isolated from the sediment by the strong chemocline, shows a more
 645 homogeneous U isotopic composition much closer to the oceanic input.

646 The depth profiles for the U isotope data in Fig. 2 clearly point to further minor processes,
647 especially near the chemocline. For example, there is clear but minor isotope exchange with
648 particulate material in July 2013 (Fig. 2) when the dissolved U pool situated just above the
649 chemocline was isotopically light, probably due to the degradation of particulate organic
650 matter with isotopically light U, similar to observed in sediment traps from Saanich Inlet
651 (Holmden et al., 2015). But the above discussion clearly suggests that the first-order process
652 governing U removal at Lake Rogoznica, in common with the Black Sea and despite the
653 higher water column sulfide concentrations, is via U diffusion downward into sediments
654 followed by reductive U precipitation with a net U isotope fractionation of +0.6‰. The
655 dominance of this first-order U removal process should, therefore, be reflected in the
656 authigenic U and its isotope composition imprinted on the sediment.

657

658 ***4.2.2 Mass balance for U and its isotopes in the lake system***

659 In principle, a diffusive removal flux for U can be calculated if the depth of U removal in the
660 pore-waters is known (e.g. Bender, 1990). This estimate could establish whether the U
661 diffusion rate across the sediment-water interface rate is fast enough to account for the
662 observed U accumulation rate in the sediments. However, the pore water data at hand are not
663 at high enough resolution to allow this calculation – the required diffusive flux dictates an e-
664 folding lengthscale for pore water removal of about 0.2 cm. On the other hand, the U isotope
665 composition of the accumulated authigenic U should reflect that dictated by the diffusive U
666 flux model if this represents the main U removal term. Thus, the $^{238}\text{U}/^{235}\text{U}$ of authigenic U in
667 sediment is expected to be ~0.6‰ heavier than the overlying bottom waters (see
668 supplementary text). At Lake Rogoznica, the average $\delta^{238}\text{U}$ of bottom waters for the six
669 sampling campaigns is $-0.94 \pm 0.07\text{‰}$ (1SD), while the average authigenic sediment

670 composition is $-0.30 \pm 0.07\text{‰}$ (1SD). The difference is in good agreement with the diffusion-
671 driven removal scenario, confirming this process as the main U removal mechanism.

672 In general, if U is to be removed by the U diffusion process from an infinitely large (or
673 rapidly replenished) water column with an open ocean composition (-0.4‰) the $\delta^{238}\text{U}$ of
674 authigenic U is expected to be $\sim +0.2\text{‰}$. At the other extreme, if the U removal flux is
675 significantly larger than the replenishment rate, thus fully depleting the water column in U,
676 sedimentary authigenic U should equal the input. These systematics reflect the degree of
677 restriction of the system, and are explored in Fig. 7 for Rogoznica and other semi-restricted
678 anoxic basins for which data are available (Kyllaren Fjord, Black Sea, Saanich Inlet, Cariaco
679 Basin, see Table 1). Fig. 7 highlights a clear relationship between the U concentration in the
680 lake bottom waters with the authigenic $\delta^{238}\text{U}$ in the sediments (open symbols and blue line).
681 This suggests that the dominant U removal mechanism - U diffusion and reduction within the
682 sediments - was the same in each semi-restricted basin. This includes the Saanich Inlet, in
683 contrast to a previous study (Anderson et al. 1989b) that suggested that the diffusive removal
684 U flux was of insufficient size to be the dominant source of authigenic U in the sediments.
685 However, this latter U removal flux estimate, based on one pore water profile in the anoxic
686 part of the inlet, may have been underestimated due to a lack of representativeness of this one
687 profile or to artifacts during U porewater extraction. A shallow pore water depletion profile of
688 ~ 0.5 cm (Anderson et al 1989b), similar to that indicated for Lake Rogoznica, would be
689 required for the diffusive U flux to be the dominant U removal process in Saanich Inlet. If the
690 diffusive U flux had indeed been underestimated, this would explain the similarities between
691 authigenic U isotope data in Saanich Inlet sediments (Holmden et al., 2015) and those for
692 other semi-restricted basins, where the diffusive removal process has been shown to be
693 dominant (Figure 7). There is also a reasonably good correlation between authigenic $\delta^{238}\text{U}$
694 and water column sulfide concentrations (closed symbols, red line). If U removal is driven by

695 diffusion into sediment, a mechanistic correlation with the reduction potential of S^- is not
696 expected. But this correlation may be a more-or-less co-incidental consequence of the control
697 that deepwater overturning timescales exert on both sulfide concentrations and authigenic
698 $\delta^{238}U$. Relatively fast water overturning rates would lead to less S^- buildup in the water
699 column, replenishment of U in the water column, and authigenic $\delta^{238}U$ fractionated from open
700 ocean seawater. In contrast, relatively slow deepwater renewal rates may lead to higher S^- ,
701 slower U replenishment rates, more quantitative removal of U from the water column and
702 authigenic $\delta^{238}U$ less fractionated from open ocean seawater.

703

704 **4.3. Mass balance for U, Mo and their isotopes in Lake Rogoznica and other euxinic** 705 **basins**

706 The impact of deep water renewal rates on sediment geochemistry can be further explored in
707 the context of coupled sedimentary U and Mo concentrations and isotope systematics (Fig. 8).
708 The key difference between Mo and U is the removal mechanism in a euxinic water column,
709 with U driven by diffusion from the water column into sediment where it is fixed, while Mo is
710 scavenged by particulate material in the water column and transported to the sediment in solid
711 form. These different removal mechanisms have been used to fingerprint specific redox
712 conditions using coupled U vs. Mo enrichment systematics in sediment (e.g. Algeo and
713 Tribovillard, 2009). Thus, in a closed system where Mo and U are quantitatively removed, the
714 Mo/U ratio and the Mo and U isotope composition of the sediment should equal the input
715 from the open ocean. Such behaviour is rarely the case, however, with different euxinic basins
716 showing variable Mo/U ratios and Mo and U isotope compositions (Fig. 8). Of the euxinic
717 basins with Mo and U isotope data, only Kyllaren Fjord (Noordmann et al., 2015) shows
718 Mo/U ratios and Mo and U isotope compositions close to the open ocean, indicating near
719 quantitative uptake of both Mo and U. Sediments from the deepest part of the Black Sea

720 (Station 9 with both U and Mo isotope data; Arnold et al., 2004; Andersen et al., 2014) show a
721 Mo/U ratio significantly below the seawater value (see also Tribovillard et al., 2006; Algeo
722 and Tribovillard, 2009). This behaviour has been linked to the contrasting sedimentary output
723 mechanisms for Mo and U, and the fact that the Black Sea exhibits extreme stratification and
724 long deep water renewal times (>500 years; Algeo & Lyons, 2006), leading to deep water Mo
725 depletion from slow resupply (Algeo & Tribovillard, 2009).

726

727 At Lake Rogoznica, Mo/U ratios are, on average, about twice the seawater value (Fig. 8A).
728 Where this has been reported, including at Saanich Inlet (Russell and Morford, 2001;
729 Holmden et al., 2015; Amini et al., 2016) and in the Cariaco Basin (Arnold et al., 2004;
730 Andersen et al., 2014), it is often interpreted as evidence for Mo addition to sediment via a Fe-
731 Mn oxide “particulate shuttle” (e.g. Algeo and Tribovillard, 2009). This suggestion is
732 supported by the previous documentation of isotopically light Mo in such sediments (Fig 8B),
733 and is also consistent with light Mo isotope data at Lake Rogoznica. It is also true, however,
734 that Mo/U ratios higher than seawater are an expected feature of small reservoirs like Lake
735 Rogoznica, even in the absence of a particulate shuttle, because of the more rapid removal of
736 Mo relative to U from the water column to sediment. In fact, any measurement of the basinal
737 average Mo/U ratio of a euxinic setting must record a Mo/U ratio higher than seawater simply
738 because uranium will be lost to a greater extent by flow of water out of the basin than will
739 Mo. For a very small and simple reservoir like Lake Rogoznica, and despite uncertainties such
740 as those arising from the possible operation of a Fe-Mn oxide “particulate shuttle”, the
741 different removal rates of Mo and U are likely to give higher Mo/U than that of seawater, and
742 this is likely to be recorded in these sediments. Only in the case where the water flow through
743 the euxinic reservoir is so slow that U diffusion into sediment can keep up, will the Mo/U
744 ratio approach the seawater value. In this context, also implicit in the treatment of Algeo and

745 Tribovillard (2009), the Mo/U ratios lower than seawater in the deep, most sulfidic, portion of
746 the Black Sea only arise because of preferential stripping of Mo relative to U from younger -
747 “upstream” - waters.

748 The Lake Rogoznica isotope data show some similarities to Kyllaren Ford for $\delta^{238}\text{U}$, but the
749 low $\delta^{98}\text{Mo}$ in both the euxinic waters ($\delta^{98}\text{Mo} \sim 2.0\text{-}2.4\text{‰}$) and sediments ($\delta^{98}\text{Mo} \sim 1.6\text{-}2.2\text{‰}$),
750 and relatively high Mo/U in the sediments, all seem to require conditions occasionally, though
751 perhaps transient, when isotopically light Mo is added to the basin. The anomalously high
752 [Mo] and low $\delta^{98}\text{Mo}$ in April 2013 surface waters, characterised by the lowest $\delta^{98}\text{Mo}$ in
753 euxinic waters ($\sim 1\text{‰}$) of any of the sampling campaigns, may have caught one such transient
754 event. However, the arrows on Fig. 8B also indicate schematically how much of the paired
755 Mo-U isotope data for euxinic basins could also be rationalised in terms of (a) variable rates
756 of Mo-U removal relative to each other, possibly driven by variable sulfide concentrations
757 within and between basins, differences in water renewal rates, as well as differences in the
758 ratio of euxinic sediment-water interface (U removal) to volume of euxinic water column (Mo
759 removal); (b) a constant effective $^{238}\text{U}/^{235}\text{U}$ fractionation factor of about 0.6‰ and; (c) Mo
760 isotope fractionation during the early history of Mo removal, e.g. driven by H_2S
761 concentrations near the action point of switch for complete transformation of $\text{Mo}^{\text{VI}}\text{O}_4^{2-}$ to
762 $\text{Mo}^{\text{VI}}\text{S}_4^{2-}$ (Helz et al., 1996; Tossel et al., 2005; Nägler et al., 2011; Kerl et al., 2017),
763 followed by much more subtle fractionations under the fully euxinic conditions that old
764 waters in the Black Sea encounter (e.g. Nägler et al., 2011). Though the data for sediments
765 recovered beneath the oldest most sulfide-rich waters of the Black Sea support such a
766 scenario, we currently lack paired U-Mo isotope data from sediments deposited from younger
767 waters to fully test this schematic scenario in the Black Sea.

768

769 **5. Conclusions**

770 Data presented in this paper for the temporal variation in the marine Lake Rogoznica, for both
771 Mo and U and their isotopes, has permitted a detailed assessment of the behaviour of these
772 redox-sensitive elements in a small euxinic basin, leading to the following principle
773 conclusions.

774 • Both $\delta^{98}\text{Mo}_{\text{part-diss}}$ and $\delta^{98}\text{Mo}_{\text{sed-porewater}}$ converge towards a $\sim 0.3\%$ offset at high
775 sulfide concentrations, providing further evidence for minor Mo isotope fractionation
776 during non-quantitative Mo uptake into euxinic sediments previously suggested for the
777 Black Sea (Näglér et al. 2011). However, Lake Rogoznica also appears to see periodic
778 addition of significant quantities of isotopically light Mo to the lake waters, possibly
779 from the release of Mo from Fe-Mn oxides formed in the oxic layer.

780

781 • Uranium concentration profiles in the lake waters show clear evidence for a dominant
782 mechanism for removal from solution via U diffusion into, and precipitation within,
783 the euxinic sediments. Periods of more intense stratification lead to well-mixed
784 profiles in the oxic upper and euxinic lower layers, with diffusion across the
785 chemocline only. Furthermore, $\delta^{238}\text{U}$ in both the sediments and deep water column are
786 consistent with an effective $^{238}\text{U}/^{235}\text{U}$ fractionation of $+0.6\%$ during uptake in the
787 sediments, in line with other studied euxinic basins.

788

789 • As a result of the different uptake mechanisms of U and Mo it is likely that sediments
790 in different areas of a euxinic basin will show different Mo/U, $\delta^{238}\text{U}$ and $\delta^{98}\text{Mo}$
791 systematics. The exact Mo and U patterns represent an interplay between: (i) the size
792 of the basin; (ii) deep water renewal rates; (iii) water-column sulfide concentrations
793 and; (iv) processes related to the Fe-Mn shuttle. This study further emphasises the

794 potential of combined Mo and U systematics to provide a better understanding of the
795 redox conditions reflected in the signatures recorded in ancient sediments.

796

797 **Acknowledgments**

798 This work was supported by ETH Zürich, the Croatian Science Foundation project IP-11-
799 2013-1205, SPHERE and the European Union Seventh Framework Programme (FP7 2007-
800 2013) under grant agreement n° 291823 Marie Curie FP7-PEOPLE-2011-COFUND (The new
801 International Fellowship Mobility Programme for Experienced Researchers in Croatia -
802 NEWFELPRO), as part of the project "Using lakes to develop isotopic tools for
803 understanding ocean redox through Earth history (IsotopicRedoxTools)". GFdS is supported
804 by a Marie Skłodowska-Curie Research Fellowship under EU Horizon2020 (SOSiC; GA
805 #708407). We would like to thank the editor, C. Holmden and two anonymous reviewers for
806 constructive comments on a previous version of the manuscript.

807

808 **References**

- 809 Abe, M., Suzuki, T., Fujii, Y., Hada, M., Hirao, K., 2008. An ab initio molecular orbital study
810 of the nuclear volume effects in uranium isotope fractionations. *J. Chem. Phys.* **129**,
811 164309.
- 812 Algeo, T.J. and Lyons, T.W. (2006) Mo-total organic carbon covariation in modern anoxic
813 marine environments: implications for analysis of paleoredox and paleohydrographic
814 conditions. *Paleoceanography* **21**, 10.1029/2004PA001112.
- 815 Algeo, T.J. and Tribovillard, N. (2009) Environmental analysis of paleocenographic systems
816 based on molybdenum-uranium covariation. *Chem. Geol.* **268**, 211-225.
- 817 Amini, M. Weis, D., Soon, M. and Francois, R. (2016) Molybdenum Isotope Fractionation in
818 Saanich Inlet, British Columbia. *Goldschmidt Conference, Yokohama*, **60**.
- 819 Andersen, M., Stirling, C., Zimmermann, B. and Halliday, A. (2010) Precise determination of
820 the open ocean $^{234}\text{U}/^{238}\text{U}$ composition. *Geochem. Geophys. Geosyst.* **11**,
821 doi.org/10.1029/2010GC003318.
- 822 Andersen, M.B., Vance, D., Keech, A.R., Rickli, J. and Hudson, G. (2013) Estimating U
823 fluxes in a high-latitude, boreal post-glacial setting using U-series isotopes in soils and
824 rivers. *Chem. Geol.* **354**, 22-32.
- 825 Andersen, M.B., Romaniello, S., Vance, D., Little, S.H., Herdman, R. and Lyons, T.W.
826 (2014) A modern framework for the interpretation of $^{238}\text{U}/^{235}\text{U}$ in studies of ancient
827 ocean redox. *Earth Planet. Sci. Lett.* **400**, 184-194.
- 828 Andersen, M.B., Elliott, T., Freymuth, H., Sims, K.W., Niu, Y. and Kelley, K.A. (2015) The
829 terrestrial uranium isotope cycle. *Nature* **517**, 356-359.
- 830 Andersen, M.B., Vance, D., Morford, J.L., Bura-Nakić, E., Breitenbach, S.F.M. and Och, L.
831 (2016) Closing in on the marine $^{238}/^{235}\text{U}$ budget. *Chem. Geol.* **420**, 11-22.

832 Andersen, M.B., Stirling, C.H. and Weyer, S. (2017) Uranium isotope fractionation. *Reviews*
833 *in Mineralogy & Geochemistry* **82**, 799-850.

834 Anderson, R.F. (1987) Redox behaviour of uranium in an anoxic marine basin. *Uranium* **3**,
835 145-164.

836 Anderson, R.F., Fleischer, M.Q. and LeHurray, A.P. (1989a) Concentration, oxidation state,
837 and particulate flux of uranium in the Black Sea. *Geochim. Cosmochim. Acta* **53**,
838 2215-2224.

839 Anderson, R.F., LeHurray, A.P., Fleischer, M.Q. and Murray, W. (1989b) Uranium deposition in
840 Saanich Inlet sediments, Vancouver Island. *Geochim. Cosmochim. Acta* **53**, 2202-
841 2213.

842 Archer, C. and Vance, D. (2008) The isotopic signature of the global riverine molybdenum
843 flux and anoxia in the ancient oceans. *Nature Geoscience* **1**, 597-600.

844 Arnold, G.I., Anbar, A.D., Barling, J. and Lyons, T.W. (2004) Molybdenum isotope evidence
845 for widespread anoxia in mid-proterozoic oceans. *Science* **304**, 87-90.

846 Azrieli-Tal, I., Matthews, A., Bar-Matthews, M., Almogi-Labin, A., Vance, D., Archer, C.
847 and Teutsch, N. (2014) Evidence from molybdenum and iron isotopes and
848 molybdenum-uranium covariation for sulphidic bottom waters during Eastern
849 Mediterranean sapropel S1 formation. *Earth Planet. Sci. Lett.* **393**, 231-242.

850 Bargar, J.R., Williams, K.H., Campbell, K.M., Long, P.E., Stubbs, J.E., Suvorova, E.I.,
851 Lezama-Pacheco, J.S., Alessi, P.S., Stylo, M., Webb, S.M., Davis, J.A., Giammar,
852 D.E., Blue, L.Y. and Bernier-Latmani, R. (2013) Uranium redox transformation
853 pathways in acetate-amended sediments. *Proc. Natl. Acad. Sci. U.S.A.* **110(12)**, 4506-
854 4511.

855 Barling, J., Arnold, G.L. and Anbar, A.D. (2001) Natural mass-dependent variations in the
856 isotopic composition of molybdenum. *Earth Planet. Sci. Lett.* **193**, 447-457.

857 Barling, J. and Anbar, A.D. (2004) Molybdenum isotope fractionation during adsorption by
858 manganese oxides. *Earth Planet. Sci. Lett.* **217**, 315-329.

859 Barnes, C.E, and Cochran, J.K. (1990) Uranium removal in oceanic sediments and the
860 oceanic-U balance. *Earth Planet. Sci. Lett.* **97**, 94-101.

861 Basu, A., Stanford, R.A., Johnson, T.M ., Lundstrom, C.C . and Löffler, F.E. (2014) Uranium
862 isotopic fractionation factors during U(VI) reduction by bacterial isolates. *Geochim.*
863 *Cosmochim. Acta* **136**, 100-113.

864 Bender, M.L. (1990) The $\delta^{18}\text{O}$ of dissolved O_2 in seawater: a unique tracer of circulation and
865 respiration in the deep sea. *J. Geophys. Res., Oceans* **95**, 22242-22252.

866 Bigeleisen, J. (1996) Nuclear size and shape effects in chemical reactions. Isotope chemistry of heavy
867 elements. *J. Amer. Chem. Soc.* **118**, 3676-3680.

868 Bostick, B.C., Fendore, S. and Helz, G.R. (2003) Differential adsorption of molybdate and
869 tetrathiomolybdate on pyrite (FeS_2). *Environ. Sci. Technol.* **37**, 285-291.

870 Brennecka, G.A., Herrmann, A.D., Alego, T.J. and Anbar, A.D. (2011a) Rapid expansion of
871 oceanic anoxia immediately before the end-Permian mass extinction. *Proc. Natl. Acad.*
872 *Sci.* **108**, 17631-17634.

873 Brennecka, G.A., Wasylenki, L.E., Bargar, J.R., Weyer, S. and Anbar, A.D. (2011b) Uranium
874 isotope fractionation during adsorption to Mn-oxyhydroxides. *Environ. Sci. Technol.*
875 **45**,1370-1375.

- 876 Bura-Nakić, E., Helz, G.R., Čosović, B. and Ciglenečki, I. (2009) Reduced sulfur species in a
877 stratified seawater lake (Rogoznica Lake, Croatia); seasonal variations and evidence
878 for organic carriers of reactive sulfur. *Geochim. Cosmochim. Acta* **73**, 3738–3751.
- 879 Cheng, H., Edwards, R.L., Sehe, C.C., Polyak, V.J., Asmerom, Y., Woodhead, Y.,
880 Hellstrom, J., Wang, Y., Kong, X., Spötl, C., Wang, X. and Alexander Jr., C. (2013)
881 Improvements in ^{230}Th dating, ^{230}Th and ^{234}U half-life values, and U-Th isotopic
882 measurements by multi-collector inductively coupled plasma mass spectrometry. *Earth*
883 *Planet. Sci. Lett.* **371-372**, 82-91.
- 884 Ciglenečki, I., Janeković, I., Marguš, M., Bura-Nakić, E., Carić, M., Ljubešić, Z., Batistić, M.,
885 Hrustić, E., Dupčić, I. and Garić, R. (2015) Impacts of extreme weather events on
886 highly eutrophic marine ecosystem (Rogoznica Lake, Adriatic coast). *Cont. Shelf Res.*
887 **108**, 144-155.
- 888 Ciglenečki, I., Carić, M., Kršinić, F., Viličić, D. and Čosović, B. (2005) The extinction by
889 sulfide - turnover and recovery of a naturally eutrophic, meromictic seawater lake. *J.*
890 *Mar. Sys.* **56**, 29-44.
- 891 Clark, S.K. and Johnson, T.M. (2008) Effective isotopic fractionation factors for solute
892 removal by reactive sediments: a laboratory microcosm and slurry study. *Environ. Sci.*
893 *Technol.* **42**, 7850-7855.
- 894 Collier, R.W. (1985) Molybdenum in the Northeast Pacific Ocean. *Limnol. Oceanogr.* **30**,
895 1351-1354.
- 896 Colodner, D., Edmond, J. and Boyle, E. (1995) Rhenium in the Black Sea: comparison with
897 molybdenum and uranium. *Earth Planet. Sci. Lett.* **131**, 1-15.
- 898 Dahl, T.W., Anbar, A.D., Gordon, G.W., Rosing, M.T., Frei, R. and Canfield, D.E. (2010)
899 The behavior of molybdenum and its isotopes across the chemocline and in the

900 sediments of sulfidic Lake Cadagno, Switzerland. *Geochim. Cosmochim. Acta* **74**,
901 144-163.

902 Emerson, S.R. and Husted, S.S. (1991) Ocean anoxic and the concentration of molybdenum
903 and vanadium in seawater. *Mar. Chem.* **34**, 177-196.

904 Erickson, B.E., and Helz, G.R. (2000) Molybdenum (VI) speciation in sulphidic waters:
905 stability and lability of thiomolybdates. *Geochim. Cosmochim. Acta* **64**, 1149-1158.

906 Goldberg, T., Archer, C., Vance, D. and Poulton, S.W. (2009) Mo isotope fractionation during
907 adsorption to Fe (oxyhydr)oxides. *Geochim. Cosmochim. Acta* **73**, 6502-6516.

908 Fujii, Y., Higuchi, N., Haruno, Y., Nomura, M. and Suzuki, T. (2006) Temperature
909 dependence of isotope effects in uranium chemical exchange reactions. *J. Nucl. Sci.*
910 *Technol.* **43**, 400–406.

911 Gordon, G.W., Lyons, T.W., Arnold, G.L., Roe, J., Sageman, B.B. and Anbar, A.D. (2009)
912 When do black shales tell molybdenum isotope tales? *Geology* **37**, 535-538.

913 Helz, G.R., Miller, C.V., Charnock, J.M., Mosselmans, J.F.W., Patrick, R.A.D., Garner, C.D.
914 and Vaughan, D.J. (1996) Mechanism of molybdenum removal from the sea and its
915 concentration in black shales: EXAFS evidence. *Geochim. Cosmochim. Acta* **60**, 3631-
916 3642.

917 Helz, G.R., Bura-Nakić, E., Mikac, N. and Ciglencčki, I. (2011) New model for molybdenum
918 behavior in euxinic waters. *Chem. Geol.* **284**, 323-332.

919

920 Herrmann, A.D., Kendall, B., Alego, T.J., Gordon, G.W., Wasylenki, L.E., and Anbar, A.D.
921 (2012) Anomalous molybdenum isotope trends in Upper Pennsylvanian euxinic facies:
922 Significance for use of ⁹⁸Mo as a global marine redox proxy. *Chem. Geol.* **324-325**,
923 87-98.

924 Hinojosa, J.L., Stirling, C.H., Reid, M.R., Moy, C.M. and Wilson, G.S. (2016) Trace metal
925 cycling and $^{238}\text{U}/^{235}\text{U}$ in New Zealand's fjords: Implications for reconstructing global
926 paleoredox conditions in organic-rich sediments. *Geochim. Cosmochim. Acta* **179**, 89-
927 109.

928 Holmden, C., Amini, M. and Francois, R. (2015) Uranium isotope fractionation in Saanich
929 Inlet: A modern analog study of a paleoredox tracer. *Geochim. Cosmochim. Acta* **153**,
930 202-215.

931 Kerl, C.F., Lohmayer, R., Bura-Nakić, E., Vance, D. and Planer-Friedrich, B. (2017)
932 Experimental confirmation of isotope fractionation in thiomolybdates using ion
933 chromatography and detection by multi-collector ICP-MS. *Anal. Chem.* **89**, 3123-
934 3129.

935 Klinkhammer, G.P. and Palmer, M.R. (1991) Uranium in the oceans: where it goes and why.
936 *Geochim. Cosmochim. Acta* **55**, 1799-1806.

937 Kowalski, et al. (2013): Pelagic molybdenum concentration anomalies and the impact of
938 sediment resuspension on the molybdenum budget in two tidal systems of the North
939 Sea. *Geochim. Cosmochim. Acta*, 119, 198-211. [dx.doi.org/10.1016/j.gca.2013.05.046](https://doi.org/10.1016/j.gca.2013.05.046)

940
941 Ku, T.L., Knauss, K.G. and Mathieu, G.G. (1977) Uranium in open ocean: concentration and
942 isotopic composition. *Deep-Sea Res.* **24**, 1005-1017. McLennan, S.M. (2001)
943 Relationships between the trace element composition of sedimentary rocks and upper
944 continental crust. *Geochem. Geophys. Geosyst.* **2**, doi: 10.1029/2000GC000109.

945 Lovley, D.R., Phillips, E.J.P., Gorby, Y.A., Landa, E.R., 1991. Microbial Reduction of
946 Uranium. *Nature* 350, 413-416. McManus, et al. (2002): Oceanic molybdenum isotope
947 fractionation: Diagenesis and hydrothermal ridge-flank alteration. *Geochemistry,*
948 *Geophysics, Geosystems*, 3 (12), 1078, doi:10.1029/2002GC000356, 2002.

- 949 McManus, J., Berelson, W.M., Klinkhammer, G.P., Hammond, D.E. and Holm, C. (2005)
950 Authigenic uranium: relationship to oxygen penetration depth and organic carbon rain.
951 *Geochim. Cosmochim. Acta* **69**, 95-108.
- 952 McManus, J., Berelson, W.M., Severmann, S., Poulson, R.I., Hammond, D.E., Klinkhammer,
953 G.P. and Holm, C. (2006) Molybdenum and uranium geochemistry in continental
954 margin sediments: paleoproxy potential. *Geochim. Cosmochim. Acta* **70**, 4643-4662.
- 955 Millero, F.J. (1986) The thermodynamic and kinetics of the hydrogen sulfide system in natural
956 waters. *Mar. Chem.* **18**, 121-147.
- 957 Montoya-Pino, C., Weyer, S., Anbar, A.D., Pross, J., Oschmann, W., van de Schootbruuge, B.
958 and Arz, H.W (2010) Global enhancement of ocean anoxia during Anoxic Oceanic
959 Event 2: A quantitative approach using U isotopes. *Geology* **38**, 315-318.
- 960 Morford, J.L. and Emerson, S. (1999) The geochemistry of redox sensitive trace metals in
961 sediments. *Geochim. Cosmochim. Acta* **63**, 1735-1750.
- 962 Nägler, T.F., Neubert, N., Böttcher, M.E., Dellwig, O. and Schnetger, B. (2011) Molybdenum
963 isotope fractionation in pelagic euxinia: Evidence from the modern Black and Baltic
964 Seas. *Chem. Geol.* **289**, 1-11.
- 965 Nägler, T.F., Anbar, A.D., Archer, C., Goldberg, T., Gordon, G.W., Greber, N.D., Siebert, C.,
966 Sohrin, Y. and Vance, D. (2014) Proposal for an international molybdenum isotope
967 measurement standard and data representation. *Geostand. Geoanal. Res.* **38**, 149-151.
- 968 Nakagawa, Y., Takano, S., Firdaus, M.L., Norisuye, K., Hirata, T., Vance, D. and Sohrin, Y.
969 (2012) The molybdenum isotopic composition of the modern ocean. *Geochem. J.* **46**,
970 131-141.
- 971 Noordmann, J., Weyer, S., Montoya-Pino, C., Dellwig, O., Neubert, N. and Eckert, S. (2015)
972 Uranium and molybdenum isotope systematics in modern euxinic basins: Case studies

973 from the central Baltic Sea and the Kyllaren fjord (Norway). *Chem. Geol.* **396**, 182-
974 195.

975 Poulson, R.L., Siebert, C., McManus, J., Severmann, S. and Berelson, W.M. (2006)
976 Authigenic molybdenum isotopes signatures in marine sediments. *Geology*, **34**, 617-
977 620.

978 Poulson Brucker, R.L., McManus, J., Severmann, S. and Berelson, W.M. (2009)
979 Molybdenum behavior during early diagenesis: insights from Mo isotopes. *Geochem.*
980 *Geophys. Geosyst.* **10**, doi:10.1029/2008GC002180.

981 Prospero, J. M. (1996). Saharan dust transport over the North Atlantic Ocean and
982 Mediterranean: an overview. In *The impact of desert dust across the Mediterranean*
983 (eds. Guerzoni, S. and Chester R.). Netherlands, Springer, pp. 133-151.

984 Richter, S., Alonso-Munoz, A., Eykens, R., Jacobsson, U., Kuehn, H., Verbruggen, A.,
985 Aregbe, Y., Wellum, R. and Keegan, E. (2008). The isotopic composition of natural
986 uranium samples-Measurements using the new n(²³³U)/n(²³⁶U) double spike IRMM-
987 3636. *Int. J. Mass Spectrom.* **269**, 146-148.

988 Rolison, J.M., Stirling, C.H., Middag, R. and Rijkenberg, M. J.A. (2017) Uranium stable
989 isotope fractionation in the Black Sea: modern calibration of the ²³⁸U/²³⁵U paleo-redox
990 proxy. *Geochim. Cosmochim. Acta* **203**, 69-88.

991 Russell, A.D. and Morford, J.L. (2001) The behaviour of redox-sensitive metals across a
992 laminated - massive-laminated transition in Saanich Inlet, British Columbia. *Marine*
993 *Geology.* **174**, 341-354.

994 Scheiderich, K., Zerkle, A.L., Helz, G.R., Farquhar, J. and Walker, R.J. (2010) Molybdenum
995 isotope, multiple sulfur isotope, and redox sensitive element behavior in early
996 Pleistocene Mediterranean Sapropels. *Chem. Geol.* **279**, 134-144.

- 997 Scott, C., Lyons, T.W., Bekker, A., Shen, Y., Poulton, S.W., Chu, X. and Anbar, A.D. (2008)
998 Tracing the stepwise oxygenation of the Proterozoic ocean. *Nature* **452**, 456-459.
- 999 Siebert, C., Nägler, T.F., von Blanckenburg, F. and Kramers, J.D. (2003) Molybdenum
1000 isotope records as a potential new proxy for paleocenography. *Earth Planet. Sci. Lett.*
1001 **211**, 159-171.
- 1002 Siebert, C., McManus, J., Bice, A., Poulson, R. and Berelson, W.M. (2006) Molybdenum
1003 isotope signatures in continental margin marine sediments. *Earth Planet. Sci. Lett.*
1004 **241**, 723-733.
- 1005 Stirling, C.H., Andersen, M.B., Potter, E.K. and Halliday, A.N. (2007) Low temperature
1006 isotopic fractionation of uranium. *Earth Planet. Sci. Lett.* **264**, 208-225.
- 1007 Stirling, C.H., Andersen, M.B., Warthmann, R. and Halliday, A.N. (2015) Isotope
1008 fractionation of ^{238}U and ^{235}U during biologically-mediated uranium reduction.
1009 *Geochim. Cosmochim. Acta* **163**, 200-218.
- 1010 Stylo, M., Neubert, N., Wang, Y., Monga, N., Romaniello, S.J. and Weyer, S. (2015)
1011 Uranium isotopes fingerprint biotic reduction. *Proc. Natl. Acad. Sci.* **112**, 5619-5624.
- 1012 Taylor, R.N. and McLennan, S. (1985) *The Continental Crust: Its Composition and Evolution.*
1013 Blackwell, Boston.
- 1014 Tissot, F.L.H. and Dauphas, N. (2015) Uranium isotopic compositions of the crust and ocean:
1015 age corrections, U budget and global extent of modern anoxia. *Geochim. Cosmochim.*
1016 *Acta* **167**, 113-143.
- 1017 Tossell, J.A. (2005) Calculating the partitioning of the isotopes of Mo between oxidic and
1018 sulfidic species in aqueous solution. *Geochim. Cosmochim. Acta* **69**, 2981-2993.

- 1019 Tribovillard, N., Alego, T., Lyons, T.W. and Riboulleau, A. (2006) Trace metals as
1020 paleoredox and paleoproductivity proxies: an update. *Chem. Geol.* **232**, 12-32.
- 1021 Tribovillard, N., Alego, T.J., Baudin, F. and Riboulleau, A. (2012) Analysis of marine
1022 environmental conditions based on molybdenum - uranium covariation - Applications
1023 to Mesozoic paleocenography. *Chem. Geol.* **324-325**, 46-58.
- 1024 Vogelín, A.R., Nägler, T.F., Samankassou, E. and Villa, I.M. (2009) Molybdenum isotopic
1025 composition of modern and Carboniferous carbonates. *Chem. Geol.* **265**, 488-498.
- 1026 Vogelín, R.A., Nägler, T.F., Beukes, N.J. and Lacassie, J.P. (2010) Molybdenum isotopes in
1027 late Archean carbonate rocks: Implications for early Earth oxygenation. *Precambrian*
1028 *Res.* **182**, 70-82.
- 1029 Vogelín, A.R., Pettke, T., Greber, N.D., von Niderhäuser, B. and Nägler, T. (2014) Magma
1030 differentiation fractionates Mo isotopes ratios: evidence from the Kos Plateau Tuff
1031 (Aegean Arc). *Lithos* **190-191**, 440-448.
- 1032 Vorlíček, T.P., and Helz, G.R. (2002) Catalysis by mineral surfaces: implications for Mo
1033 geochemistry in anoxic environments. *Geochim. Cosmochim. Acta* **66**, 3679-3692.
- 1034 Wang, X., Johnson, T.M. and Lundstrom, C.C., 2015. Isotope fractionation during oxidation
1035 of tetravalent uranium by dissolved oxygen. *Geochim. Cosmochim. Acta* **150**, 160–
1036 170.
- 1037 Westermann, S., Vance, D., Cameron, V., Archer, C. and Robinson, S.A. (2014)
1038 Heterogeneous oxidation states in the Atlantic and Tethys oceans during Oceanic
1039 Anoxic Event 2. *Earth Planet. Sci. Lett.* **404**, 178-189.
- 1040 Weyer, S., Anbar, A.D., Gerdes, A., Gordon, G.W., Alego, T.J. and Boyle, E.A. (2008)
1041 Natural fractionation of $^{238}\text{U}/^{235}\text{U}$. *Geochim. Cosmochim. Acta* **72**, 345-359.

1042 Zheng, Y., Anderson, R.F., van Geen, A., Fleischer, M.Q., 2002. Preservation of particulate
1043 non-lithogenic uranium in marine sediments. *Geochimica et Cosmochimica Acta* 66,
1044 3085-309
1045

1046 **Figure captions**

1047 **Figure 1:** Depth–time sections for salinity, oxygen, sulfide, and particulate Fe and Mn
1048 concentrations in Lake Rogoznica during 2013 (February, April, July and October) and
1049 2015 (April and July).

1050 **Figure 2:** Depth profiles of dissolved (salinity normalised) and particulate Mo and U
1051 concentrations, dissolved and particulate $\delta^{98}\text{Mo}$ and $\delta^{238}\text{U}$. The very high Mo
1052 concentration at the surface (0 m) in April and July 2013, as well as the low $\delta^{238}\text{U}$ in July
1053 2013 (7.5 m), are given as numerical values.

1054 **Figure 3:** Authigenic sedimentary and pore water Mo and U concentrations, as well as
1055 $\delta^{98}\text{Mo}$ and $\delta^{238}\text{U}$, in the sediment core recovered from the anoxic portion of Lake
1056 Rogoznica, plotted versus depth beneath the sediment water interface. The dashed lines
1057 on all four plots show the isotopic composition of the open ocean for Mo and U.

1058 **Figure 4:** A: Mo isotopic composition plotted against reciprocal Mo concentration for all
1059 samples with $\text{O}_2 > 5\text{mg l}^{-1}$. Most data fall along a flat trajectory close to oceanic Mo
1060 isotope ratios at variable Mo concentrations (horizontal grey arrow). Some data for April
1061 and July 2013, however, show higher Mo concentrations and lower $\delta^{98}\text{Mo}$, lying along a
1062 trajectory that requires an extra source of Mo with $\delta^{98}\text{Mo}$ around +0.4 to +0.5‰. B:
1063 $\delta^{98}\text{Mo}_{\text{diss-part}}$ for all dissolved-particulate pairs, including sediment-pore water, for
1064 samples where sulfide is detectable. The water column data appear to become asymptotic
1065 to a value around +0.3‰ at very high dissolved sulfide concentrations. Though pore
1066 water data are more scattered, no $\delta^{98}\text{Mo}_{\text{diss-part}}$ is below this value.

1067 **Figure 5:** A: Salinity-normalised [U] data from the February 2013 campaign (red diamonds);
1068 the modelled thick black line on the diagram is for a virtually stagnant lake (no advection) in
1069 which U diffuses downwards into the sediment. The relative importance of advection versus

1070 diffusion is represented by the value of ω/D , which is ~ 0.007 for the modelled evolution. For
1071 comparison, the thin dashed line shows a profile dominated by advection, with a $\omega/D = 0.7$,
1072 two orders of magnitude greater. B: All data from the four intermediate sampling campaigns.
1073 C: Data from the July 2015 campaign (purple circles). The water column is separated into two
1074 rather isolated layers above and below the chemocline. The black curve shows the impact of
1075 transport within each layer that is completely dominated by advection over diffusion ($\omega/D =$
1076 2 ± 0.3) - both reservoirs are well mixed for [U] with much slower communication across the
1077 chemocline.

1078 **Figure 6:** Salinity-normalised [U] vs. $\delta^{238}\text{U}$ for Lake Rogoznica. A: Data from the February
1079 2013 campaign (red diamonds), which, as for [U] (Fig 5), most closely follow the expected
1080 trajectory for diffusion-driven U removal from a stagnant water column. The red dotted line is
1081 a regression of the data (based on $1/[\text{U}]$ vs $\delta^{238}\text{U}$). The curved solid black line shows the
1082 approximate trajectory expected for the waters, with diffusion-driven U removal with a
1083 $+0.6\%$ difference in the removal rate constants for ^{238}U and ^{235}U , and a starting composition
1084 similar to water sample with the highest [U] (see supplementary text for details). The dashed
1085 line shows the trajectory for removal within the water column via a Rayleigh process with a
1086 1.2% fractionation in $^{238}\text{U}/^{235}\text{U}$, starting from the same water sample as the diffusion model.
1087 B: All data from the four intermediate sampling campaigns. C: Data for July 2015 (purple
1088 circles) which, again like the [U] data (Fig 5), show strong asymmetry. This profile is
1089 characterised by an upper oxic layer that is near homogeneous in [U] and $\delta^{238}\text{U}$ because of
1090 isolation from the sediment by a strong chemocline, and a lower anoxic layer. The [U]- $\delta^{238}\text{U}$
1091 systematics in the lower anoxic layer ($1/[\text{U}]$ vs $\delta^{238}\text{U}$ regression; dotted line) follow the model
1092 trajectory for diffusion-driven U removal from a stagnant water column (solid line), with the
1093 deepest oxic sample, nearest the chemocline, used as the upper boundary for both the
1094 regression line and diffusion modelling.

1095 **Figure 7:** Relationship between $\delta^{238}\text{U}_{\text{auth}}$ and (i) the percentage of dissolved U removal in
1096 deep anoxic vs surface water (bottom axis, open symbols, blue regression line) and (ii) total
1097 dissolved sulfide (ΣS^{2-}) in the anoxic part of the water column (closed symbols, red regression
1098 line). Sulfide concentrations in Supplementary Table 2. See Table 1 for citations to data. The
1099 slope of the U removal vs. $\delta^{238}\text{U}_{\text{auth}}$ best fit regression line is close to that expected for
1100 diffusive removal U flux with an effective $^{238}\text{U}/^{235}\text{U}$ fractionation $\sim+0.6$ (see supplementary
1101 text).

1102 **Figure 8:** A: U vs Mo enrichment factors and, B: authigenic $\delta^{98}\text{Mo}$ vs. $\delta^{238}\text{U}$, for Lake
1103 Rogoznica sediments (individual sediment horizons, open circles; average, filled circle)
1104 compared to other euxinic basins. Key to colours for both panels as indicated in Panel B. Data
1105 sources: Kyllaren Fjord (Noordmann et al., 2015), Black Sea (Station 9 data in Arnold et al.,
1106 2004; Andersen et al., 2014), Cariaco Basin (Arnold et al., 2004; Andersen et al., 2014),
1107 Saanich Inlet (Russell and Morford, 2001; Holmden et al., 2015; Amini et al., 2016). In A the
1108 seawater Mo/U is plotted as the solid line, with deviations from the seawater ratio shown as
1109 dashed lines as indicated. In B schematic solid arrows show how sediment deposited beneath
1110 euxinic waters would vary in different euxinic basins for high versus low rates of Mo removal
1111 relative to U, assuming a constant fractionation factor for uranium isotopes. These scenarios
1112 would require Mo fractionation during initial non-quantitative removal to be substantial, but
1113 more subtle during the subsequent more quantitative removal, consistent with theoretical,
1114 experimental and observational constraints (e.g. Helz et al., 1996; Tossel, 2005; Nagler et al.,
1115 2011; Kerl et al., 2017).

1116

1117

1118

1119

1120

1121
1122

1123 **Table 1:** $[\Sigma S^{-II}]$, $[U]_{diss}$ and $\delta^{238}U$ of dissolved ($\delta^{238}U_{diss}$) and authigenic sedimentary ($\delta^{238}U_{auth}$)
 1124 uranium in the anoxic water columns and sediments of different modern anoxic basins.

Euxinic basin	Salinity norm. $[U]_{diss}$ nmol l ⁻¹ **	$\delta^{238}U_{auth}$ in sediments	$\delta^{238}U_{diss}$ deep waters	$[\Sigma S^{-II}]$ $\mu\text{mol l}^{-1}$ deep waters	Source
Lake Rogoznica*	2.8/***	-0.30	-0.94	1214	This work
Kyllaren Fjord	7.5/12.9	-0.22	-0.71	4316	Noordmann et al. (2015)
Black Sea	9.3/17.3	-0.03	-0.68	262	Rolison et al. (2016)
Cariaco Trench	12.0/14.5	+0.03	-	40	Anderson (1987) Emerson and Husted (1991) Andersen et al. (2014)
Saanich Inlet	14.7/15.4	+0.17	-0.48	30	Emerson and Husted (1991) Holmden et al. (2015)

1125 *average values for $[U]_{diss}$, $\delta^{238}U_{auth}$, $\delta^{238}U_{diss}$, and ΣS^{-II} in the deepest anoxic Lake Rogoznica samples from all 6
 1126 sampling events.

1127 *Salinity normalised (35) U concentrations for deep waters/surface waters. This ratio is used for the U water
 1128 column removal fraction in Figure 7.

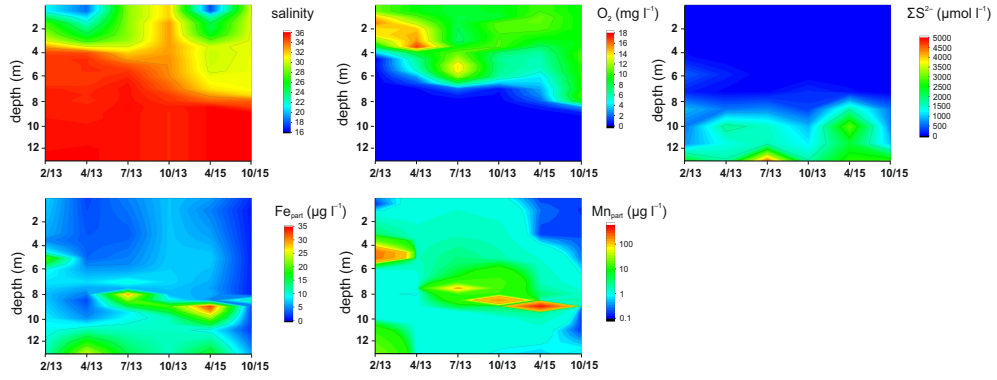
1129 ***A [U] as the open ocean was used for the surface waters (13.4 nmol⁻¹) in this setting.

1130

1131

1132

Figure 1

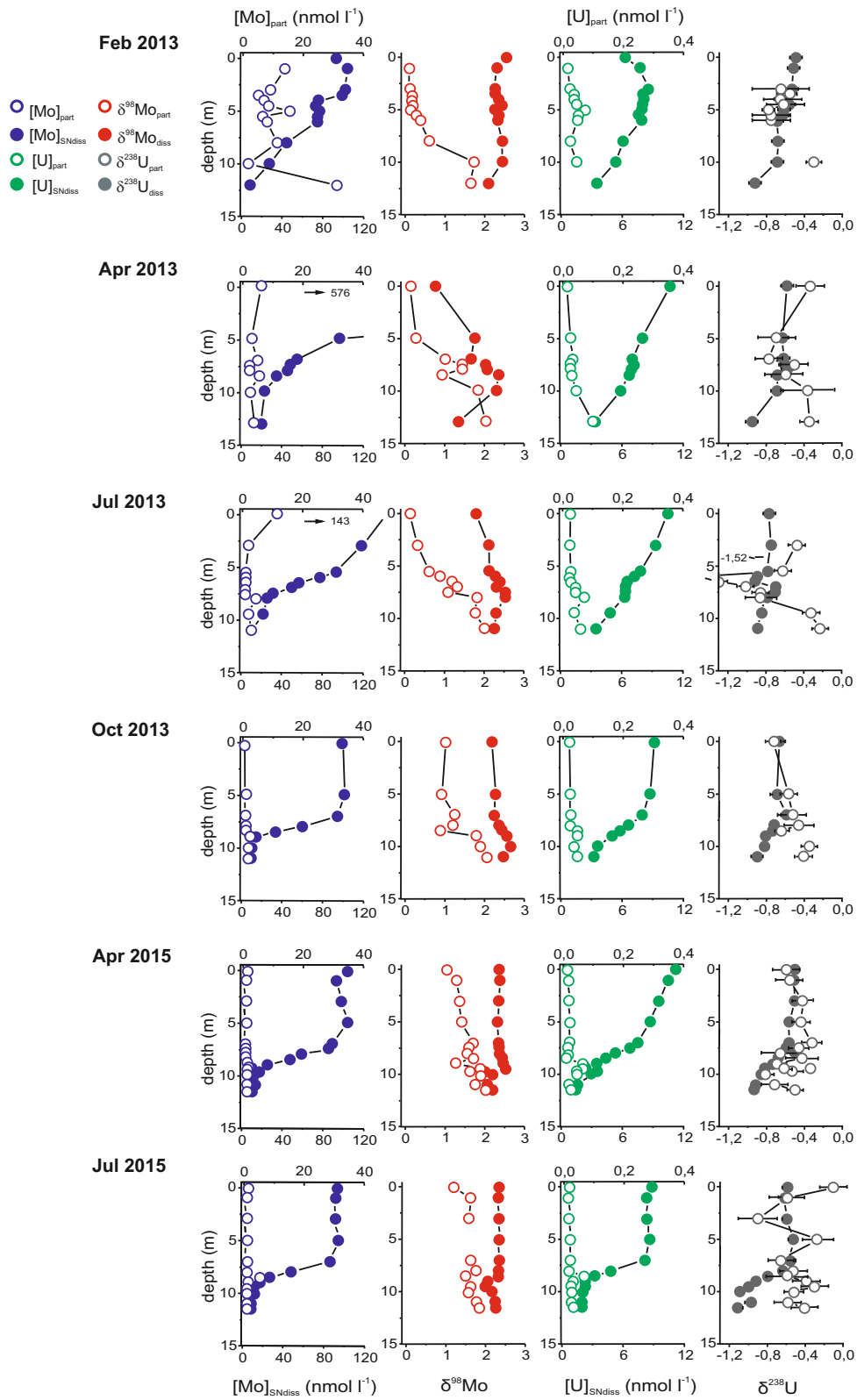


1133

1134

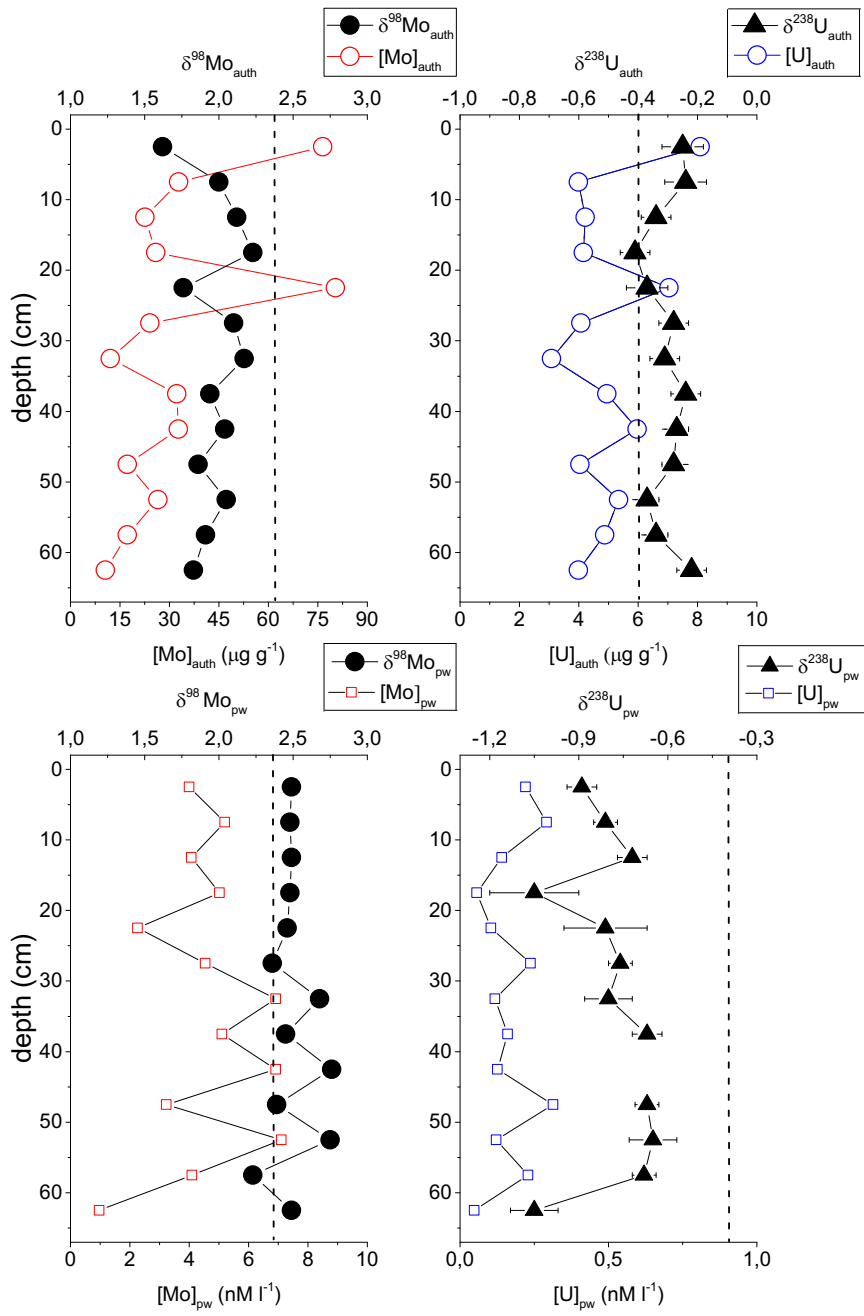
1135

Figure 2



1140

Figure 3



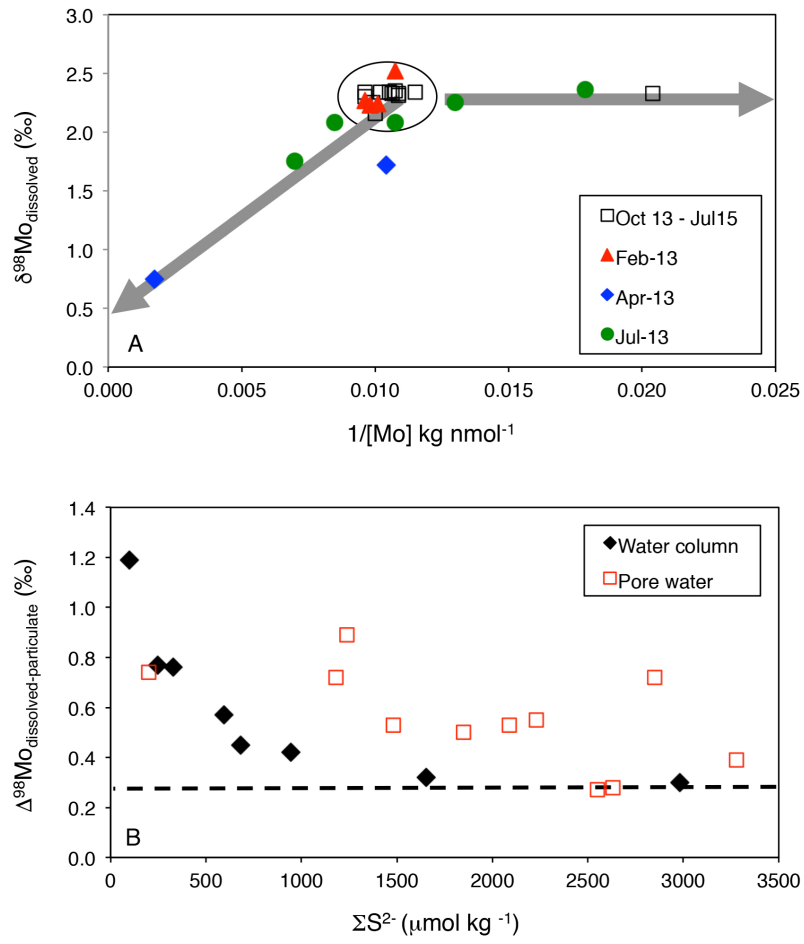
1141

1142

1143

1144

Figure 4



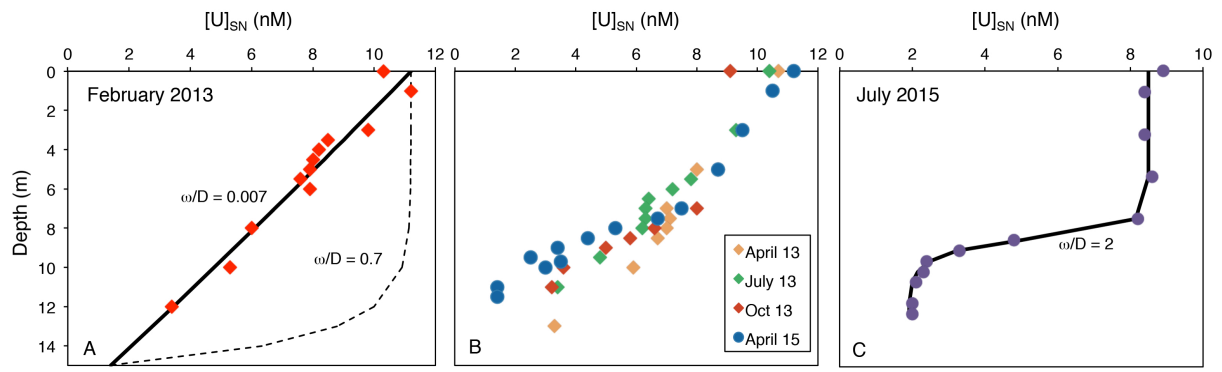
1145

1146

1147

1148

Figure 5



1149

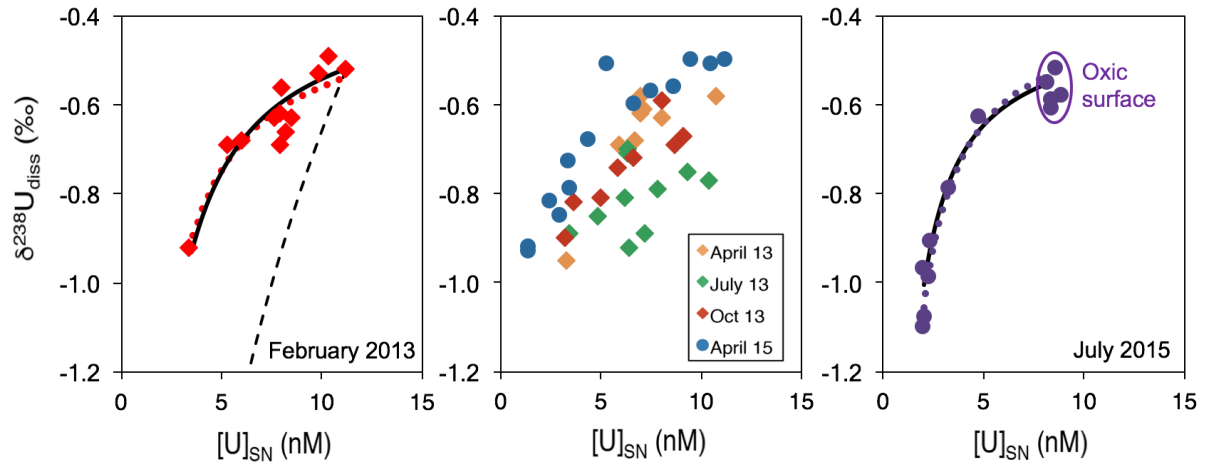
1150

1151

1152

1153

Figure 6



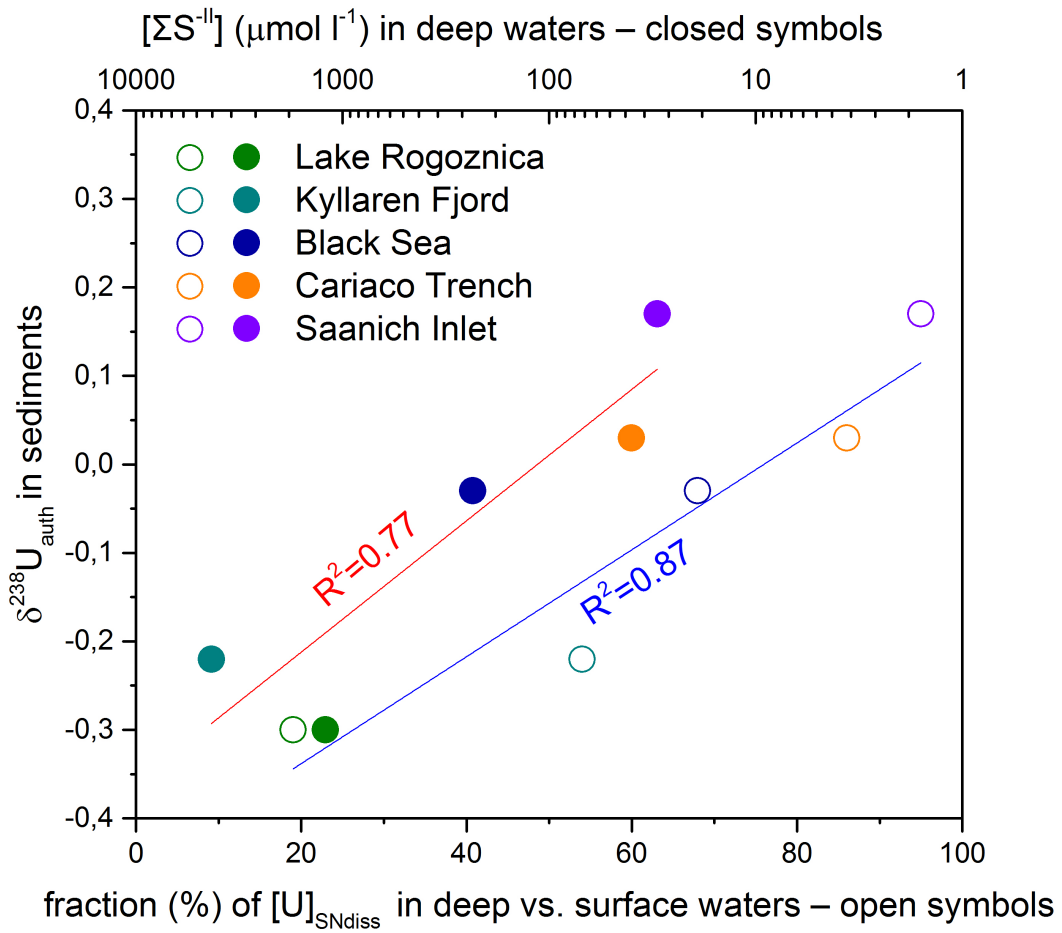
1154

1155

1156

Figure 7

1157



1158

1159

1160

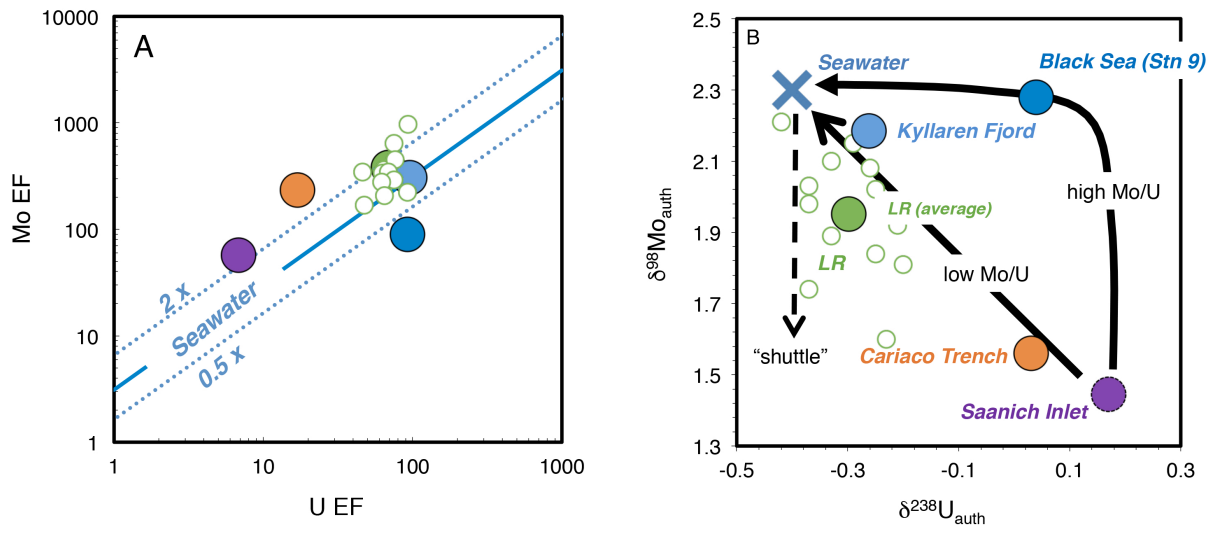
1161

1162

1163

Figure 8

1164



1165

1166

1167

1168

1169 **Supplementary text to ‘Coupled Mo-U abundances and isotopes in a small**
1170 **marine euxinic basin: constraints on processes in euxinic basins’ by Bura-**
1171 **Nakic et al.**

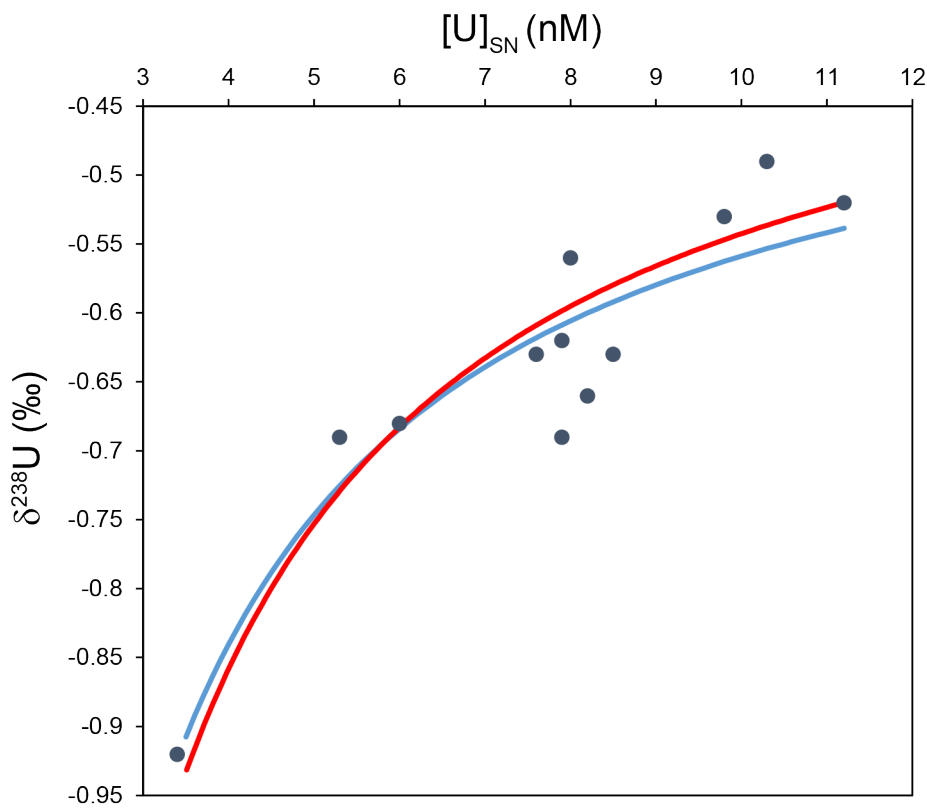
1172

1173 We constructed a simple one-dimensional water-column model in order to assess the
1174 covariation between [U] and $\delta^{238}\text{U}$ expected, when U is only removed from the very bottom
1175 of the water column (by diffusion into sediment) with an effective isotope effect of +0.6‰.
1176 For simplicity, the model only considers the well-mixed portion of the water column above
1177 the sediments, such that we need only consider non-directional mixing processes within the
1178 water column and can ignore unidirectional advective transport. We do this by discretizing the
1179 water column into a series of 0.1m-high cells, each of which exchanges a constant volume
1180 flux (v) with its immediate neighbours. Uranium is transported conservatively within the
1181 water column, and lost only from the lowermost cell of the simulated water column. The
1182 model carries tracers of ^{235}U and ^{238}U , and the isotope fractionation associated with loss to
1183 sediments is represented as a differential first-order rate constant (k) for these two tracers.

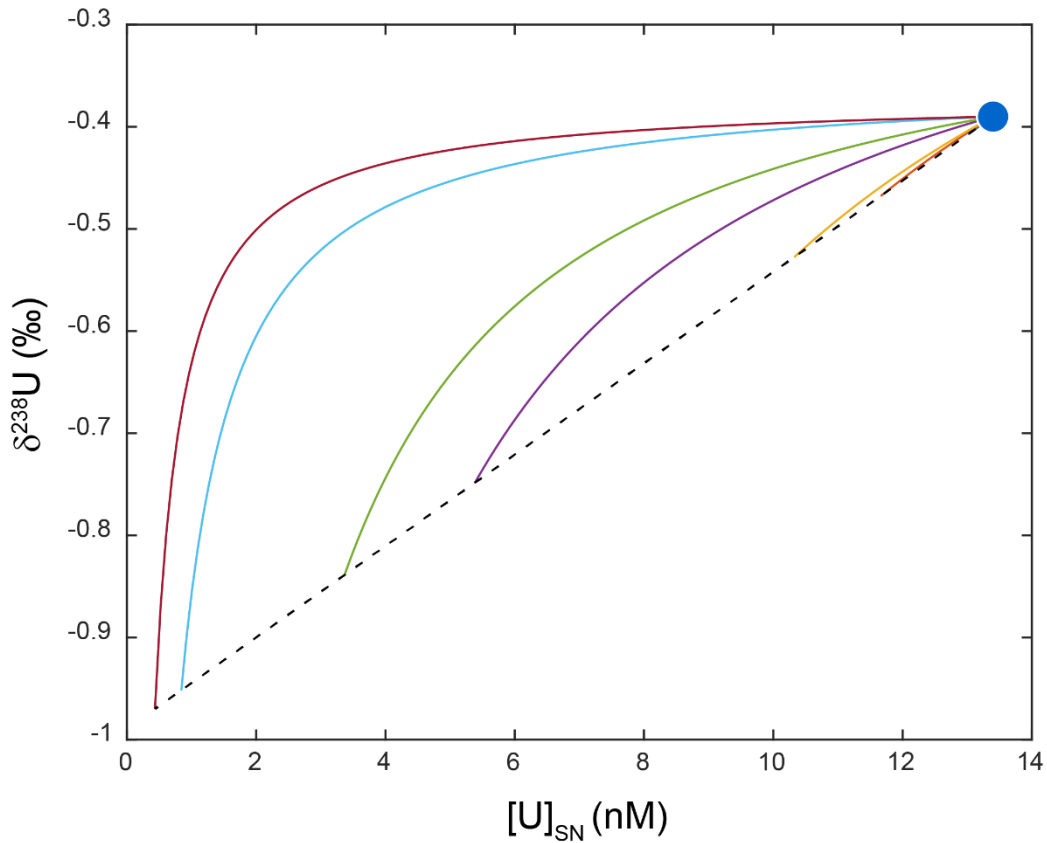
1184

1185 Our model can be applied to the entire 15m depth of Lake Rogoznica in February 2013, when
1186 [U] decreases near-linearly with depth and can be well described by a water column
1187 dominated by diffusion (see Section 4.2.1 and Fig. 5 of the main text). In order to compare the
1188 model result to the data, the surface boundary condition of the model is initialised with [U]
1189 and $\delta^{238}\text{U}$ values observed at the top of the water column in February 2013. The simulated [U]
1190 and $\delta^{238}\text{U}$ profiles depend on the ratio of the exchange flux v to the loss rate-constant k . We
1191 set this ratio so as to reproduce the observed [U] gradient in February 2013 (Fig. S1); the
1192 model simulates the corresponding $\delta^{238}\text{U}$ profile expected when U is lost from the very
1193 bottom of the water column with an isotope effect of +0.6‰. As can be seen in Fig. S1, (and
1194 Fig. 6A of the main manuscript), the model reproduces the observed co-variation between [U]
1195 and $\delta^{238}\text{U}$. Interestingly, the simulated co-variation is essentially identical to the mixing trend
1196 predicted by linear regression of $\delta^{238}\text{U}$ against $1/[\text{U}]$ (blue line in Fig. S1). Simulating U-loss
1197 to sediment with an isotope effect of +0.6‰ is thus sufficient to reproduce the degree of $\delta^{238}\text{U}$
1198 variation and observed co-variation between [U] and $\delta^{238}\text{U}$. It is important to reiterate that the
1199 model result is independent of the numerical values of v and k , being instead controlled by the
1200 ratio between them, which sets the [U] gradient across the water column.

1201 More generally, the model can be applied to study the U isotope systematics of well-mixed
 1202 euxinic water columns in which U is lost to sediment via diffusion. In Fig. S2, we show
 1203 results in which the model was initialized with the [U] and $\delta^{238}\text{U}$ characteristics of open-ocean
 1204 seawater ($[\text{U}] = 13.4\text{nM}$ and $\delta^{238}\text{U} = -0.39\text{‰}$), and the degree of U drawdown at the base of
 1205 the water column was varied by changing v/k . The predicted co-variation trend between [U]
 1206 and $\delta^{238}\text{U}$ becomes increasingly non-linear as U loss to the sediment increases. However, it is
 1207 important to note that the $\delta^{238}\text{U}$ of dissolved U at the very base of the water column is a
 1208 simple linear function of the degree to which U is drawn down by loss to sediment, relative to
 1209 the initial open-ocean condition.
 1210



1211
 1212 **Fig. S1: U isotope systematics of Lake Rogoznica in February 2013.** When initialised with
 1213 the observed [U] and $\delta^{238}\text{U}$ properties of the top of the water column (top right), the one-
 1214 dimensional water column model (red line) reproduces the degree of $\delta^{238}\text{U}$ variability
 1215 expected when [U] is drawn down to ~ 3.5 nM at the base of the water column, due to
 1216 diffusion-driven loss to the sediments. The model solution is virtually indistinguishable from
 1217 a linear regression to the data ($\delta^{238}\text{U}$ versus $1/[\text{U}]$) that describes the co-variation expected
 1218 purely as the result of conservative mixing of U within the water column (blue line).



1219
 1220
 1221
 1222
 1223
 1224
 1225
 1226
 1227
 1228

Fig. S2: U isotope systematics for varying degrees of U drawdown. Each curve represents the water-column co-variation between $[U]$ and $\delta^{238}U$ predicted by the model for varying degrees of U drawdown at the base of the water column with an isotope effect of $+0.6\text{‰}$. The starting point (blue circle) represents open-ocean seawater. As can be seen, this relationship becomes increasingly non-linear as the $[U]$ difference between the top and bottom of the water column increases. However, the isotope composition of dissolved U at the very base of the water column is a simple linear function of $[U]$, i.e. of the extent to which U has been drawn down relative to the open-ocean initial of 13.4 nM.